© 2020. Published by The Company of Biologists Ltd | Journal of Cell Science (2020) 133, jcs234104. doi:10.1242/jcs.234104

RESEARCH ARTICLE

The atypical Rho GTPase RhoU interacts with intersectin-2 to regulate endosomal recycling pathways

Olga Gubar[1,2], Pauline Croisé[1], Sergii Kropyvko[2], Tetyana Gryaznova[2], Petra Tóth[1], Anne Blangy[3], Nicolas Vitale[1], Alla Rynditch[2], Stéphane Gasman[1,*] and Stéphane Ory[1,*,‡]

ABSTRACT

Rho GTPases play a key role in various membrane trafficking processes. RhoU is an atypical small Rho GTPase related to Rac/Cdc42, which possesses unique N- and C-terminal domains that regulate its function and its subcellular localization. RhoU localizes at the plasma membrane, on endosomes and in cell adhesion structures where it governs cell signaling, differentiation and migration. However, despite its endomembrane localization, RhoU function in vesicular trafficking has been unexplored. Here, we identified intersectins (ITSNs) as new binding partners for RhoU and showed that the second PxxP motif at the N terminus of RhoU mediated interactions with the SH3 domains of ITSNs. To evaluate the function of RhoU and ITSNs in vesicular trafficking, we used fluorescent transferrin as a cargo for uptake experiments. We showed that silencing of either RhoU or ITSN2, but not ITSN1, increased transferrin accumulation in early endosomes, resulting from a defect in fast vesicle recycling. Concomitantly, RhoU and ITSN2 colocalized to a subset of Rab4-positive vesicles, suggesting that a RhoU–ITSN2 interaction may occur on fast recycling endosomes to regulate the fate of vesicular cargos.

KEY WORDS: Atypical Rho GTPases, Intersectins, Vesicle recycling, SH3 domains, Proline-rich domains

INTRODUCTION

Rho GTPases are small G proteins belonging to the Ras superfamily. They regulate many cell functions including cell migration, cell polarity and cell proliferation (Jaffe and Hall, 2005). Although most studies have been focused on the role of the canonical members of the family, namely RhoA, Rac1 and Cdc42, evidence has emerged for critical functions of the so-called atypical Rho GTPases, which encompass Rnd, RhoH, RhoU, RhoV and RhoBTB proteins (Aspenström et al., 2007). Atypical Rho GTPases are mostly found associated with membranes and in a constitutively active state due to high guanine nucleotide exchange rate (RhoU, RhoV) or due to amino acid substitutions that render them defective for GTPase activity (Rnd proteins, RhoH). Activities of atypical Rho GTPases are primarily regulated by the balance between transcription and translation, degradation, and binding to regulatory proteins. Indeed, compared to canonical members, most atypical Rho GTPases possess additional domains at their N and/or C terminus that bind various proteins and contribute to regulation of their activities (Aspenström et al., 2007; Vega and Ridley, 2008).

The atypical Rho GTPase RhoU was first isolated as a gene transcriptionally upregulated in wnt-1-transformed mouse mammary epithelial cells (Tao et al., 2001). RhoU shares significant homology with Cdc42, as well as some biological functions. For example, RhoU binds and activates p21-activated kinase (PAK1), induces filopodia and regulates cell tight junctions (Brady et al., 2009; Garrard et al., 2003; Saras et al., 2004; Tao et al., 2001). In addition, amino acids of the effector loop that mediate binding to downstream targets such as PAK1 or Par6 are conserved between RhoU and Cdc42 (Brady et al., 2009; Ory et al., 2007). However, RhoU possesses N- and C-terminal extensions that confer unique properties. The N-terminal extension is enriched in proline residues and mediates binding to SH3-domain-possessing proteins such as Nck1 and Grb2 (Saras et al., 2004; Shutes et al., 2004). Deletion of the N-terminal extension increases RhoU transforming activity as well as RhoU signaling through PAK1 activation (Berzat et al., 2005; Brady et al., 2009). Moreover, mutations of the proline-rich motifs of RhoU impair EGF receptor signaling by preventing RhoU recruitment by Grb2 to the EGF receptor complex (Zhang et al., 2011). Whereas its activity appears to be regulated by its N-terminal extensions, RhoU subcellular localization is mostly controlled by its 21-amino-acid-long C-terminal extension, which contains a non-conventional CAAX box (Berzat et al., 2005) and its effector loop (Ory et al., 2007). RhoU has been found to localize at the plasma membrane, on endosomes and at focal adhesions where it regulates their turnover (Chuang et al., 2007; Ory et al., 2007). The association of RhoU with membranes is mostly dependent on its CAAX motif (Berzat et al., 2005; Zhang et al., 2011), whereas a bipartite motif comprising the C-terminal extension and the effector loop is needed for targeting to focal adhesions (Ory et al., 2007). Collectively, these studies have revealed that the N- and C-terminal extensions of RhoU have distinct functions, the first regulating RhoU activity, and the second contributing to RhoU subcellular localization.

To further characterize RhoU and its function, we searched for new binding partners in pulldown experiments and found that intersectins (ITSNs) formed a complex with RhoU. Because ITSNs are multidomain endocytic proteins mostly involved in clathrin-mediated endocytosis pathways (Tsyba et al., 2011), we next investigated the importance of RhoU and ITSNs in the transferrin trafficking pathway and found that RhoU and ITSN2 coordinate the recycling of transferrin receptors.

RESULTS

ITSN1 and ITSN2 interact with RhoU

Preliminary data based on GST–RhoU pulldown experiments combined with mass spectrometry analysis suggested that the short form of intersectin-2 (ITSN2-S), a member of the ITSN family, could interact

[1]Centre National de la Recherche Scientifique, Université de Strasbourg, Institut des Neurosciences Cellulaires et Intégratives, F-67000 Strasbourg, France. [2]Institute of Molecular Biology and Genetics NASU, 150 Zabolotnogo Street, Kyiv 03680, Ukraine. [3]Centre de Recherche en Biologie Cellulaire de Montpellier (CRBM), Univ. Montpellier, CNRS, 34000 Montpellier, France.
*These authors contributed equally to this work

‡Author for correspondence (ory@inci-cnrs.unistra.fr)

O.G., 0000-0001-5224-7118; S.K., 0000-0002-2685-080X; T.G., 0000-0002-6479-4861; A.B., 0000-0001-7043-0784; N.V., 0000-0002-4752-4907; S.G., 0000-0001-8415-1276; S.O., 0000-0003-4359-1157

Handling Editor: Michael Way
Received 8 May 2019; Accepted 21 July 2020

Journal of Cell Science (2020) 133, jcs234104. doi:10.1242/jcs.234104

with RhoU (S.O. and A.B., unpublished). Moreover, bioinformatics analysis to find potential RhoU-binding motifs, using the Scansite database (http://scansite3.mit.edu; Obenauer et al., 2003), identified the SH3A domain of ITSN1 with the highest predicted binding score, whereas the SH3 domain of Nck1, a known partner of RhoU (Shutes et al., 2004), had the second highest score (Fig. S1). This potential interaction between RhoU and ITSN isoforms was further investigated using GST pulldown and immunoprecipitation experiments (Fig. 1). intersectin proteins are encoded by two genes, *ITSN1* and *ITSN2*, and both proteins exist in at least one short (S) and one long (L) form resulting from alternative splicing (Fig. 1A)

To validate the potential formation of a complex between RhoU and ITSN2-S, we first performed pulldown experiments using purified recombinant GST–RhoU with cell extracts from HEK293T cell lines expressing GFP–ITSN2-S. Western blot analysis using anti-GFP antibodies revealed that ITSN2-S precipitated with GST–RhoU (Fig. 1B). As a truncated mutant of ITSN2-S with its SH3 domains deleted (Nt-ITSN2; Fig. 1A) was not precipitated by GST–RhoU, the formation of a complex between RhoU and ITSN2 is most likely mediated through one or several SH3 domains (Fig. 1B). To determine which of the five SH3 domains of ITSN2 could be involved, pulldown experiments were performed using individual SH3 domains fused to GST. As illustrated in Fig. 1C, only the GST–SH3E domain fusion precipitated myc–RhoU from HEK293T cell extracts, suggesting that RhoU binds specifically to the SH3E domain of ITSN2 and not to the others. To further demonstrate that the RhoU–ITSN2 interaction occurs in cells, we performed immunoprecipitation experiments in HEK293T cells expressing myc–RhoU. Both endogenous ITSN2-S and 2-L were co-immunoprecipitated by myc–RhoU, suggesting that both forms of ITSN2 were associated with RhoU in cells (Fig. 1D). Moreover, in line with our database analysis suggesting that RhoU possesses a potential ITSN1 binding site, ITSN1-S and ITSN1-L also co-precipitated with myc–RhoU in HEK293T cells, demonstrating that RhoU can interact with both ITSN1 and ITSN2 (Fig. 1E).

Finally, GST pulldown experiments using all five (SH3A–E) or individual SH3 domains of ITSN1 showed that SH3A, -C, and -E efficiently precipitated RhoU whereas SH3B and -D did not (Fig. 1F), suggesting that the SH3 domains also mediated the interaction between ITSN1 and RhoU. Altogether, these *in vitro* experiments indicated that specific SH3 domains of ITSN1 and ITSN2 form a complex with RhoU.

N-terminal proline-rich domains of RhoU mediate binding to SH3 domains of ITSNs

RhoU has been classified as an atypical Rho protein, notably because of additional domains found at its N- and C-terminal regions compared to its close homolog Cdc42 (Aspenström et al., 2007; Shutes et al., 2004). The RhoU N-terminal extension possesses two PxxPxR sequences (where x indicates any amino acid) corresponding to consensus SH3-binding motifs (Shutes et al., 2004; Yu et al., 1994). To identify which proline-rich motif of RhoU is important for binding to ITSN SH3 domains, we expressed RhoU mutants in which proline to alanine substitutions were introduced into individual (M1 or M2) or both (DM) proline-rich motif sequences (Fig. 2A). These mutations have been previously shown to disrupt RhoU binding to SH3 domains of the adaptor protein Grb2 (Zhang et al., 2011). We performed pulldown assays with SH3A–E of ITSN1 on cell lysates of HEK293T cells expressing myc–RhoU and found that M1 mutations only slightly reduced RhoU binding, whereas M2 and DM mutations completely abolished it indicating that the second proline-rich motif of RhoU is the main binding site for ITSN1 SH3 domains (Fig. 2B). To confirm that the proline-dependent interaction also occurred in cells, the myc–RhoU mutants were co-expressed with Omni-tagged ITSN1 in HEK293T to conduct a co-immunoprecipitation experiment. In agreement with pulldown experiments, amounts of ITSN1 co-immunoprecipitated with RhoU were dramatically reduced with the M2 and DM mutations, whereas M1 mutations had only a modest effect (Fig. 2C). Similar pulldown experiments were performed using the SH3A–E domains of ITSN2, showing that M2 and DM mutants were unable to bind the ITSN2 SH3 domains (Fig. 2D). Taken together, these data indicate that the second proline-rich motif of the RhoU N-terminal extension constitutes the preferential binding site for the SH3 domains of ITSN proteins.

ITSN2 and RhoU are involved in the transferrin receptor trafficking pathway

ITSN proteins have been mostly studied in the context of clathrin-mediated endocytosis, where they participate in maturation of clathrin-coated pits (CCPs) (Henne et al., 2010; Praefcke et al., 2004; Tsyba et al., 2011). Moreover, RhoU has been localized to early endosomes (Zhang et al., 2011), a major sorting platform of endocytic pathways. Together with our *in vitro* observations, this suggests that RhoU and ITSN2 might be involved in the same pathway to regulate endocytosis and/or recycling of cargo engaged in the clathrin-mediated endocytic pathways. To test this hypothesis, we examined whether transferrin (Tf) endocytic and recycling pathways were altered following depletion of ITSN or RhoU proteins by siRNA (Fig. 3A). First, using flow cytometry, we evaluated Tf endocytosis by continuously feeding HeLa cells depleted for ITSN1, ITSN2 or RhoU for 15 min at 37°C with Alexa-Fluor-647-labeled Tf (Tf–A647). After stripping off Tf–A647 bound to the cell surface, we measured mean fluorescence intensity of endocytosed Tf–A647. This assay allows for monitoring the overall Tf pathway at equilibrium, including Tf endocytosis and recycling. Interestingly, we observed a modest but significant increase in Tf–A647 uptake following depletion of ITSN2 or RhoU (Fig. 3B). In contrast, depletion of ITSN1 had no effect (Fig. 3B). As a control, clathrin heavy chain (CLTC) depletion showed that clathrin-dependent endocytosis was efficiently inhibited in our assays (Fig. 3B). To gain further insight into the subcellular route altered, we next set up a fluorescence-based image analysis to quantify levels of Tf–A647 in both cells and vesicles. In agreement with our flow cytometry experiments, HeLa cells fed for 15 min with Tf–A647 showed increased amounts of Tf upon either ITSN2 or RhoU silencing, as compared to those in control or ITSN1-knockdown cells (Fig. 3D). Interestingly, Tf-positive vesicles were more dispersed in cells silenced for RhoU compared to control cells, whereas there was no significant change in Tf distribution in ITSN1- or ITSN2-knockdown cells (Fig. 3C; Fig. S2). This observation raises the question of whether RhoU or ITSN2 might alter clathrin-mediated endocytosis pathways. To probe for this, we analyzed EGF receptor endocytosis by incubating cells with a low concentration of fluorescent EGF (EGF–TRITC) to favor clathrin-dependent endocytosis of the EGF receptors (Sigismund et al., 2008). As previously described (Martin et al., 2006), after 15 min endocytosis, ITSN1 silencing reduced EGF–TRITC uptake by 50% compared to uptake by control cells (Fig. 3E). Interestingly, ITSN2 silencing moderately reduced EGF–TRITC endocytosis, whereas RhoU silencing had no effect (Fig. 3E), indicating that the increase of ligand–receptor endocytosis after ITSN2 or RhoU silencing was restricted to transferrin. Because RhoU and ITSN2 proteins interacted and regulated Tf trafficking, we next looked at the subcellular distribution of RhoU and ITSN2 co-expressed in HeLa cells. In agreement with previous studies (Henne et al., 2010; Pucharcos et al., 2000), HA–ITSN2-L localized to small puncta at the

Journal of Cell Science (2020) 133, jcs234104. doi:10.1242/jcs.234104

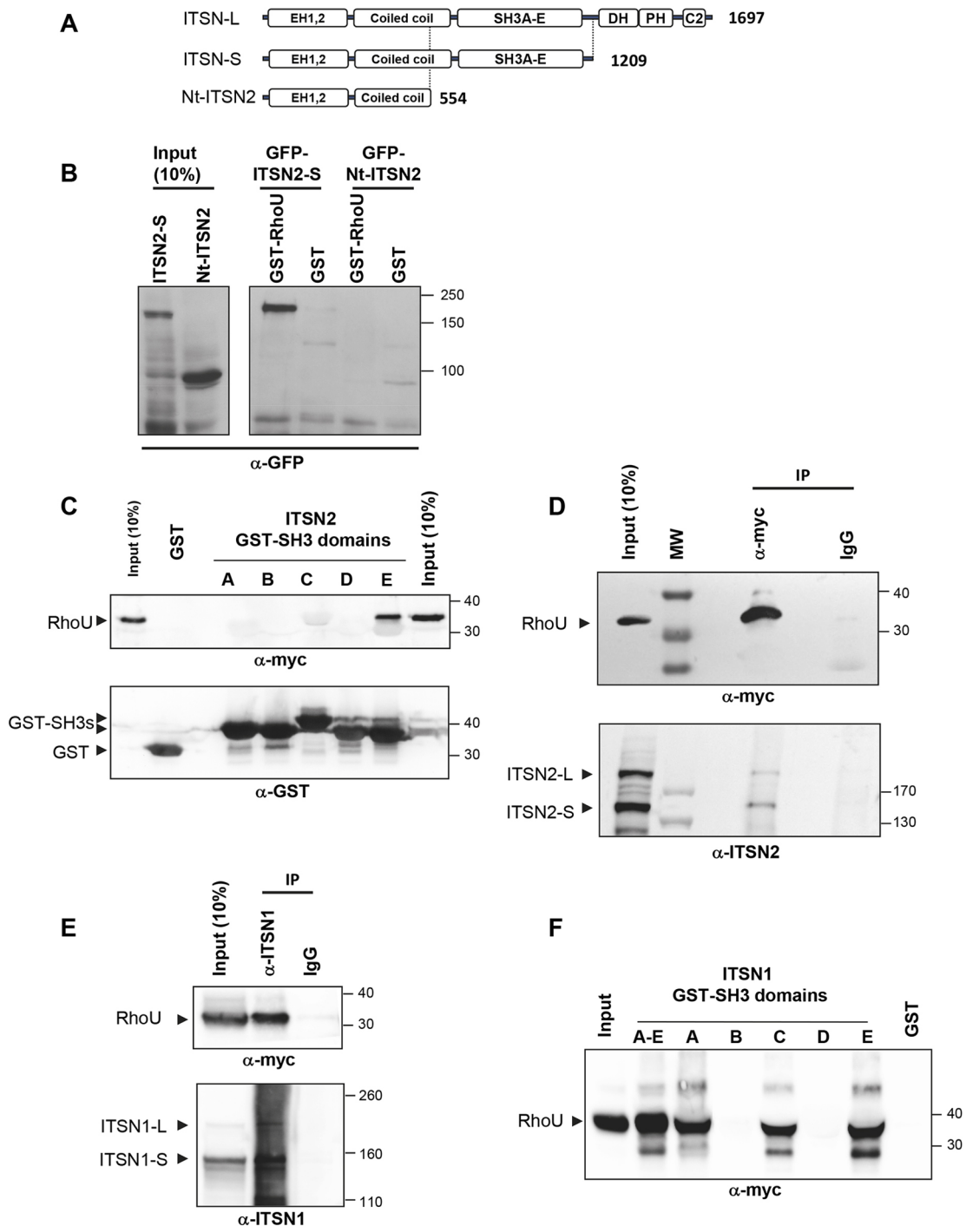

Fig. 1. RhoU interacts with ITSN proteins. (A) Schematic representation of the intersectin isoforms. Both short (ITSN-S) and long (ITSN-L) forms contain two Epsin homology domains (EH1, EH2), a coiled-coil domain and five Src homology 3 domains (SH3A–E), whereas only the long form (ITSN-L) contains three additional domains, a Dbl homology domain (DH) catalyzing the activation of Cdc42, a pleckstrin homology domain (PH) needed for plasma membrane targeting and a C2 domain. Nt-ITSN2 contains EH domains and a truncated coiled-coil domain. Numbers indicate amino acid length of encoded proteins. (B) HEK293T cells were transfected with GFP–ITSN2-S or GFP–Nt-ITSN2, and lysates subjected to pulldown experiments using either recombinant GST or GST–WT RhoU. Precipitated proteins were revealed by western blotting using anti-GFP antibodies. (C) Pulldown experiments using individual SH3 domains (SH3A to SH3E) of ITSN2 fused to GST and lysates of HEK293T cells expressing myc–RhoU. Precipitated RhoU was revealed by western blotting with anti-myc antibodies, and GST fusion proteins with anti-GST antibodies. (D) Immunoprecipitation (IP) experiments from lysates of cells expressing myc-tagged RhoU using anti-myc antibodies. Arrowheads point to both forms of precipitated endogenous ITSN2 (ITSN2-S and ITSN2-L). MW indicates molecular mass markers. (E) Immunoprecipitation of endogenous ITSN1 from HEK293T cells transfected with myc-tagged RhoU. Precipitated RhoU was revealed using anti-myc antibodies. Arrowheads point to both forms of ITSN1 (ITSN1-S and ITSN1-L). (F) HEK293T cells were transfected with myc-tagged WT RhoU and cell lysates were incubated with GST alone, GST fused to individual SH3 domain (SH3A to SH3E) or to the five SH3 domains (SH3A–E) of ITSN1. Precipitated RhoU was revealed by western blotting with anti-myc antibodies. Molecular masses indicated in B–F are in kDa.

Journal of Cell Science (2020) 133, jcs234104. doi:10.1242/jcs.234104

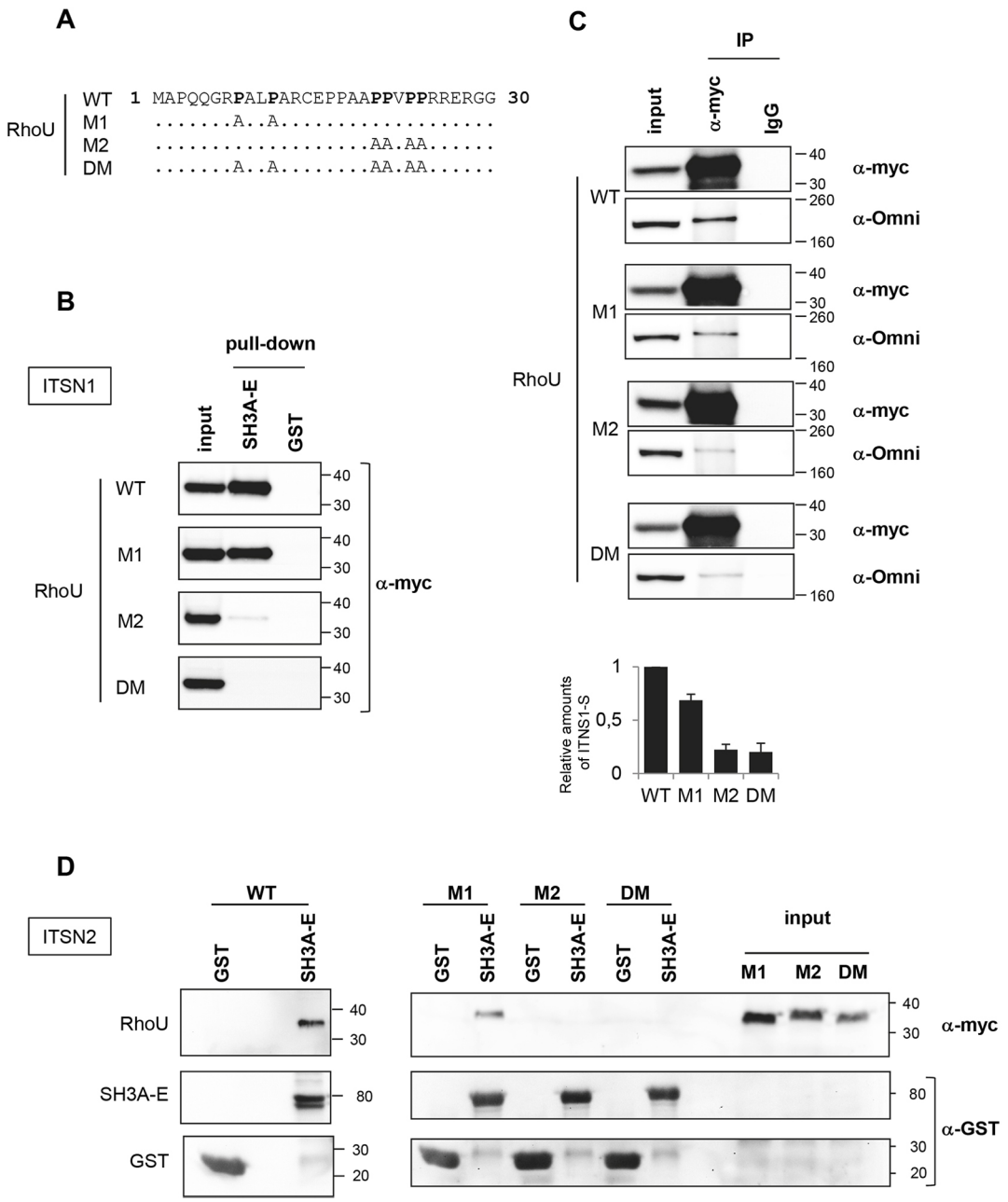

Fig. 2. Proline-rich motifs of RhoU mediate the interaction with SH3 domains of ITSNs. (A) Schematic representation of RhoU proline-rich mutants used. Proline to alanine substitutions are indicated. (B) Lysates from cells expressing either WT, M1, M2 or DM RhoU mutants were incubated with either GST alone or GST fused to the five SH3 domains of ITSN1 (SH3A–E). Precipitated RhoU was revealed by western blotting using anti-myc antibodies. (C) Co-immunoprecipitation experiments from lysates of cells expressing myc-tagged RhoU and Omni-tagged ITSN1-L. Myc-tagged RhoU was immunoprecipitated (IP) using anti-myc antibodies and associated ITSN1 was revealed by western blotting. Relative amounts of precipitated ITSN1 are shown on the graph. Data are mean±s.e.m. of three independent experiments. (D) GST or GST–SH3A–E domains of ITSN2 were used on lysates from cells expressing WT RhoU and the indicated RhoU mutants. Precipitated RhoU and recombinant proteins were revealed by western blotting using anti-myc and anti-GST antibodies, respectively. In B–D, input lanes are 10% of total lysate, and molecular masses indicated are in kDa.

cell periphery (Fig. 3F, inset 1, arrowheads) reminiscent of CCPs. RhoU was found in linear structures at the cell periphery resembling focal adhesions (Fig. 3F, inset 1, arrows). Interestingly, neither GFP–RhoU localized to peripheral ITSN2 puncta nor ITSN2 were found at focal adhesions stained for RhoU. However, we did observe colocalization between RhoU and ITSN2 in a subset of perinuclear vesicles (Fig. 3F, inset 2, arrowheads). We could also observe ITSN2 enriched in small extensions emanating from GFP–RhoU vesicles (Fig. 3F, inset 2, arrows). Taken together, these experiments revealed the importance of RhoU and ITSN2 in the regulation of the Tf endocytic pathway.

ITSN2 and RhoU regulate transferrin receptor recycling

We next attempted to unravel how RhoU and ITSN2 act together to regulate Tf receptor trafficking. The increase in intracellular Tf reported above could result from more receptor at the cell surface and/or a delay in Tf recycling leading to accumulation of Tf in cells. To estimate the amounts of Tf receptor at the cell surface, we

Journal of Cell Science (2020) 133, jcs234104. doi:10.1242/jcs.234104

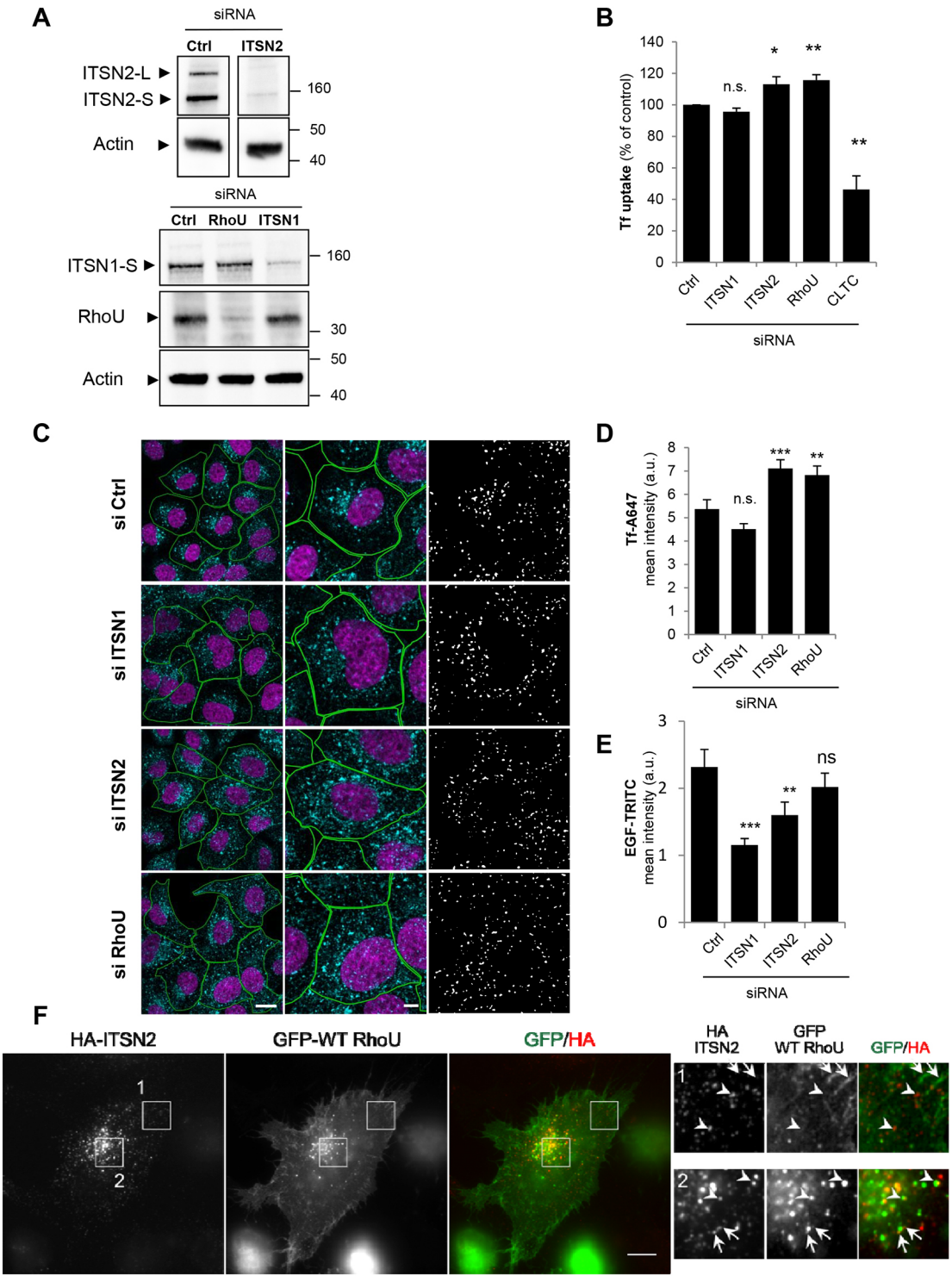

Fig. 3. See next page for legend.

incubated cells with Tf–A647 for 1 h at 4°C, a condition that blocks endocytosis. After a quick wash, amounts of bound Tf–A647 were estimated using flow cytometry (Fig. 4A). Fluorescence levels were not significantly different in HeLa cells depleted for ITSN2, RhoU or CLTC as compared to levels in the control, indicating that the higher uptake of Tf is probably not a consequence of an increase in cell surface Tf receptor. To test for a defect in Tf recycling, the surface pool of Tf receptor was labeled at 4°C with Tf–A647 for 1 h. Excess Tf–A647 was then removed, and the HeLa cells transferred to 37°C for 5, 15 or 30 min. After stripping away the surface pool of Tf–A647, amounts of intracellular Tf–A647 were estimated using flow cytometry. Interestingly, as early as 5 min after triggering endocytosis, twice the amount of Tf was endocytosed in cells depleted for ITSN2 or RhoU as compared to that endocytosed by control cells (Fig. 4B). Larger amounts of endocytosed Tf were maintained at 15 and 30 min time points, but differences were reduced, suggesting that the major trafficking defect occurs early during the transferrin receptor trafficking process.

Journal of Cell Science (2020) 133, jcs234104. doi:10.1242/jcs.234104

Fig. 3. Tf trafficking is defective in HeLa cells silenced for RhoU or ITSN2. (A) Western blot analysis of lysates from HeLa cells transfected with siRNA targeting ITSN1, ITSN2 or RhoU, compared to cells transfected with an unrelated siRNA (Ctrl). Actin is shown as a loading control and molecular masses indicated are in kDa. (B) Flow cytometry quantification of the endocytosis of transferrin. HeLa cells silenced for ITSN1, ITSN2, RhoU or clathrin heavy chain (CLTC) were serum starved for 30 min prior to incubation with Tf–A647 for 15 min. Cells were detached and the mean intensity of internalized Tf in at least 30,000 cells was determined using flow cytometry. Data are represented as mean±s.e.m. percentage of control cell uptake (n=3 experiments). (C) Left: representative field of view of cells silenced for ITSN1, ITSN2 or RhoU and subjected to 15 min fluorescent Tf uptake experiments. Nucleus (magenta) and Tf (cyan) are shown, and cell outlines are indicated. Scale bar: 10 µm. Middle: a close-up view of single cell is shown. Scale bar: 5 µm. Right: binary mask corresponding to segmented fluorescent spots of Tf-positive vesicles, generated using the wavelet spot detector in Icy software. Scale bar: 5 µm. (D) Quantification of Tf endocytosis. The sum of vesicle intensity was computed and normalized to the cell surface intensity, and the mean±s.e.m. intensity for each condition is shown on the graph. n=30 cells. (E) Quantification of EGF–TRITC endocytosis. The sum of vesicle intensity was computed and normalized to the cell surface intensity, and the mean±s.e.m. intensity for each condition is shown on the graph. n=30 cells. (F) Wide-field immunofluorescence images of HeLa cells transfected with HA–ITSN2-L and myc-tagged WT RhoU. Inset 1 shows peripheral localization of ITSN2 in puncta (arrowheads) and GFP–RhoU in focal adhesions (arrows). Inset 2 shows partial colocalization of ITSN2 and GFP–RhoU in perinuclear vesicles. Arrow and arrowheads point to vesicles with both ITSN2 and GFP–RhoU. Note that ITSN2 can be found enriched at tips of tubules emanating from a GFP–RhoU vesicle (arrows). Scale bar: 5 µm. *P<0.05; **P<0.01; ***P<0.001; n.s., not significant as compared with control (Student's t-test in B; one-way ANOVA with Holm–Sidak post-hoc test in D,E).

The increase in amount of Tf in cells could be the result of an increase in Tf uptake or a decrease in Tf recycling. Tf recycling comprises two recycling modes: a 'fast' mode involving direct recycling from early endosomes that occurs within 5 min, and a 'slow' mode, which takes place after sorting to recycling endosomes and occurs after 15 min (Ciechanover et al., 1983; Grant and Donaldson, 2009).

To discriminate between these two possibilities, we applied a method previously used, with slight modifications (Chamberland et al., 2016; Kalaidzidis et al., 2015). Because the first steps of endocytosis require roughly 2 min before fast recycling takes place (Aguet et al., 2013; Hao and Maxfield, 2000; Taylor et al., 2011), we labeled surface Tf receptor with Tf–A647 for 1 h at 4°C, then placed cells at 37°C for 2 min to stay within the limit of 'pure endocytosis'. Cell surface-bound Tf was stripped away, and amounts of endocytosed Tf were analyzed using flow cytometry. Fig. 4C shows that amounts of Tf were significantly increased in cells depleted for ITSN2 or RhoU. To estimate the defect in fast recycling, cells were returned back to 37°C for the indicated amount of time and analyzed using flow cytometry. Fig. 4D shows that the recycling defect occurs shortly after endocytosis because, compared to recycling in control cells, barely no transferrin was recycled after 2 min in cells silenced for RhoU or ITSN2. Levels of recycling increased between 2 and 5 min, and reached similar levels to those in the control at 15 min. These experiments indicate that in the absence of RhoU or ITSN2, Tf endocytosis is accelerated and fast recycling of Tf is altered. Both alterations likely contribute to the increase in intracellular Tf observed in the absence of RhoU or ITSN2.

To further show that RhoU and its binding to SH3 domain-bearing proteins is important for Tf trafficking, we performed rescue experiments by generating stable HeLa lines expressing mouse variants of myc-tagged wild-type RhoU (Mm WT RhoU) or myc-tagged DM mutant RhoU (Mm DM RhoU). Mismatches between the siRNA used to target human RhoU and the mouse RhoU sequence should render the mouse variants resistant to silencing. Several clones were isolated and screened for expression profile and subcellular distribution of mouse RhoU. Clones with moderate plasma membrane and subcellular vesicle expression were selected (WT3 and DM4; Fig. 4E). Both clones were used for endocytosis assays. As in Fig. 4B, the surface pool of Tf receptor was labeled at 4°C with Tf–A647, and cells were transferred to 37°C for 5, 15 or 30 min. After stripping away the surface pool of Tf–A647, amounts of intracellular Tf–A647 were estimated using flow cytometry. At 5 min, and as reported in Fig. 4B, twice the amount of Tf–A647 was taken up in parent cells silenced for RhoU, as compared to uptake in the control (Fig. 4F). Notably, the WT3 clone knocked-down for human RhoU showed reduced amounts of endocytosed Tf at all time points as compared to the parent cells (Fig. 4F). In contrast, the DM4 clone behaved like the parent cells, indicating that mouse RhoU is able to partially restore Tf uptake in RhoU-silenced cells only if RhoU has the ability to interact with SH3 domain-bearing proteins.

Because early endosomes are the major routing platform prior to fast or slow recycling, we sought for defects in Tf routing after a short period of endocytosis (Fig. 5). We used immunofluorescence and performed the same assay as for flow cytometry but cells were either fixed after 2 min Tf–A647 pulse (t=0 in Fig. 5) or returned back to 37°C for 2 or 5 min before fixation to analyze the fate of Tf–A647 that had been endocytosed during the 2 min pulse. We then quantified two parameters: first, we calculated the percentage of Tf-positive vesicles that colocalized with EEA1 compartments (object-based colocalization) and second, we measured the percentage of Tf–A647 found in EEA1 compartments at a given time by integrating amounts of fluorescent Tf in EEA1 compartments compared to total amounts of Tf in cells. As shown in Fig. 5A, in control cells, a small proportion of Tf-positive vesicles had already reached the EEA1 compartment at t=0. As previously reported (Kalaidzidis et al., 2015), colocalization of Tf-containing vesicles with EEA1 increased between 0 and 2 min and started to decrease between 2 to 5 min, suggesting that Tf had either been recycled or had left the EEA1 compartment to reach the recycling endosomes. In cells depleted for ITSN2 or RhoU, the proportion of Tf-containing vesicles colocalizing with EEA1 was comparable to that in control cells (Fig. 5A,B) indicating that, at the early time point, there is no major rerouting of Tf. However, when we estimated amounts of Tf in the EEA1 compartment, we found that, at 2 and 5 min, the proportion of fluorescent Tf in the EEA1 compartment was increased after depletion of ITSN2 or RhoU (Fig. 5C) suggesting that Tf residency time in EEA1 was increased in these conditions. To further analyze the fate of Tf–A647, we conducted pulse-chase experiments for 2 and 5 min and estimated amounts of Tf–A647 reaching Rab11-positive endosomes. Fig. 5D shows that, in agreement with a delay in recycling or a slowing down of vesicle maturation toward recycling endosomes, the proportion of Tf in the Rab11 compartment was higher at 2 and 15 min when ITSN2 or RhoU was silenced. Altogether, these data demonstrate that RhoU and ITSN2 regulate Tf-vesicle progression along the endocytic route and might be needed for fast recycling of Tf receptor.

RhoU is distributed along the endocytic route

RhoU has been observed to localize in cell adhesion structures and vesicular compartments (Chuang et al., 2007; Ory et al., 2007; Zhang et al., 2011). The precise distribution of RhoU along the endocytic route is, however, unknown. Because available antibodies against RhoU do not detect endogenous RhoU by immunofluorescence, we co-transfected myc–RhoU together with GFP-tagged Rab4a, -5a, -11a and -7a, several specific markers of the endocytic route (Wandinger-Ness and Zerial, 2014). RhoU was found partially

Journal of Cell Science (2020) 133, jcs234104. doi:10.1242/jcs.234104

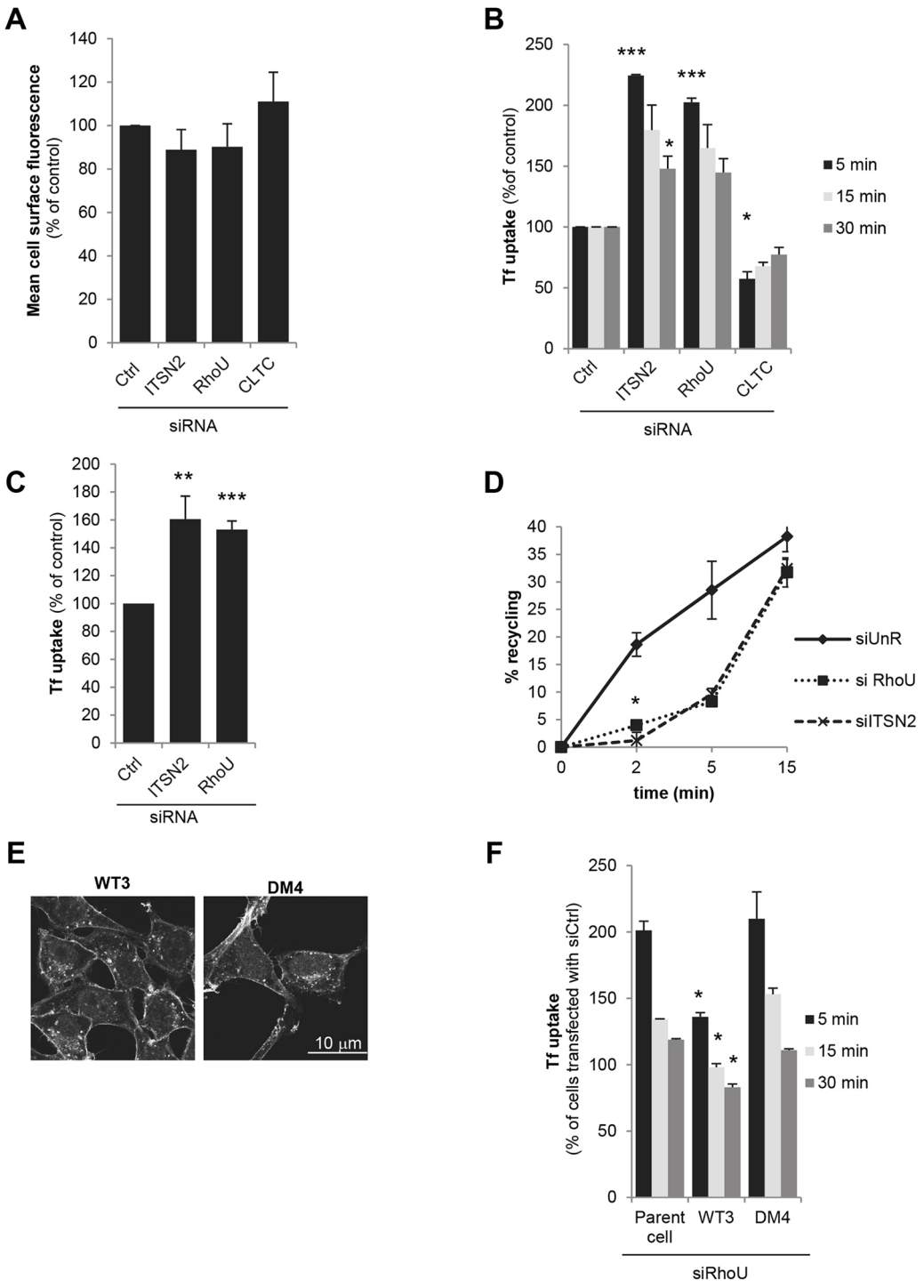

Fig. 4. Depletion of ITSN2 or RhoU alters the fast recycling pathway. HeLa cells were silenced by siRNA transfection for ITSN1, ITSN2, RhoU or clathrin heavy chain (CLTC) and compared to cells expressing an unrelated siRNA (Ctrl). (A) Flow cytometry analysis of Tf–A647 binding at the cell surface. Data are mean±s.e.m. cell surface fluorescence, expressed as a percentage of the control. *n*=3 independent experiments. (B) Timecourse of Tf–A647 endocytosis. Cells were serum starved for 30 min and incubated on ice for 1 h with Tf–A647. Cells were quickly washed and incubated for 5, 15 or 30 min at 37°C prior to flow cytometry analysis. The mean intensity of internalized Tf in at least 30,000 cells was determined and data are represented as mean±s.e.m. percentage of control cell uptake, which is set as 100% (*n*=2 experiments). (C) Transferrin uptake during a 2 min pulse. HeLa cells were incubated for 1 h at 4°C with Tf–647 before a 2min incubation at 37°C to allow for endocytosis. Plasma membrane-bound Tf–A647 was removed by acid wash, and cells were analyzed by flow cytometry. The mean intensity of internalized Tf–A647 was determined and data are represented as mean±s.e.m. percentage of control cell uptake (*n*=3 experiments). (D) Transferrin recycling assays. Following a 2 min Tf–A647 pulse, cells were acid washed to remove plasma membrane-bound Tf–A647 and incubated at 37°C for the indicated amount of time before flow cytometry analysis. The mean intensity of internalized Tf–A647 was determined and data are represented as mean±s.e.m. percentage of recycled Tf–A647 (*n*=2 experiments). siUnR, data from control cells treated with an unrelated siRNA. (E) Confocal microscopy analysis of WT3 and DM4 clones. Cells were stained for myc–RhoU using Alexa-555-conjugated anti-myc antibodies. (F) Timecourse of Tf–A647 endocytosis, performed as in B. Data are represented as mean±s.e.m. percentage of the respective cell lines transfected with Ctrl siRNA (*n*=2 experiments). **P*<0.05, ***P*<0.01, ****P*<0.001 as compared with control (Student's *t*-test).

Journal of Cell Science (2020) 133, jcs234104. doi:10.1242/jcs.234104

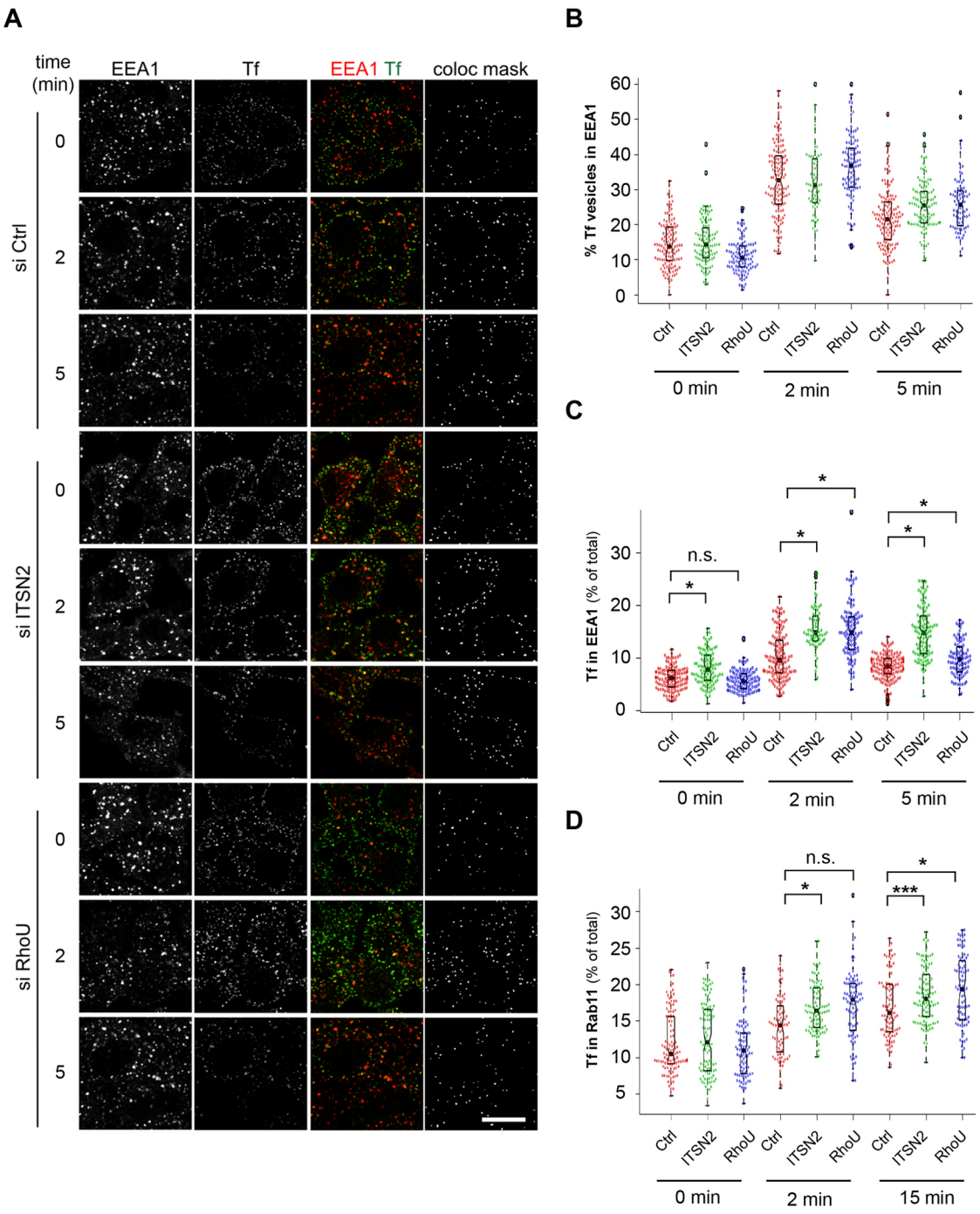

Fig. 5. Depletion of ITSN2 or RhoU leads to accumulation of Tf in EEA1 compartments. (A) Representative field of view of control HeLa cells (si Ctrl) and HeLa cells silenced for ITSN2 or RhoU, pulsed for 2 min with Tf–A647 and chased for the indicated time after stripping away cell surface Tf. Cells were stained for EEA1, and the colocalization mask between EEA1 and Tf–A647 is shown (coloc mask). The percentages of Tf-positive vesicles colocalizing with EEA1 (B), and the fraction of Tf–A647 found in EEA1-positive (C) or Rab11-positive endosomes (D) as compared to total amounts of Tf in cells were quantified over time (n=2 experiments, at least 40 cells per condition per experiment). Individual data points are shown, with median, 25% and 75% quartile indicated. To assess significance, Kruskal–Wallis on rank with Dunn's post-hoc test was performed for B and C and a one-way ANOVA with Holm–Sidak post-hoc test was performed for D. *P<0.05; ***P<0.001; n.s., not significant. Scale bar 10 µm.

colocalized with fast recycling endosomes (Rab4a), early endosomes (Rab5a) and slow recycling endosomes (Rab11a; Fig. 6A). Very weak colocalization was observed with late endosomes. Indeed, less than 10% of wild-type RhoU (WT RhoU) was found in GFP–Rab7a compartments (data not shown) as compared to around 30% of RhoU colocalized with GFP–Rab4a and GFP–Rab5a, and 50% with GFP–Rab11a (Fig. 6B). Since DM mutant RhoU (DM RhoU) is impaired in binding to ITSNs, we used this mutant to test whether the subcellular distribution of RhoU depends on its ability to interact with ITSNs. Fig. 6B shows that the distribution of DM RhoU was comparable to WT RhoU, suggesting that binding to ITSNs is dispensable for RhoU subcellular distribution.

Journal of Cell Science (2020) 133, jcs234104. doi:10.1242/jcs.234104

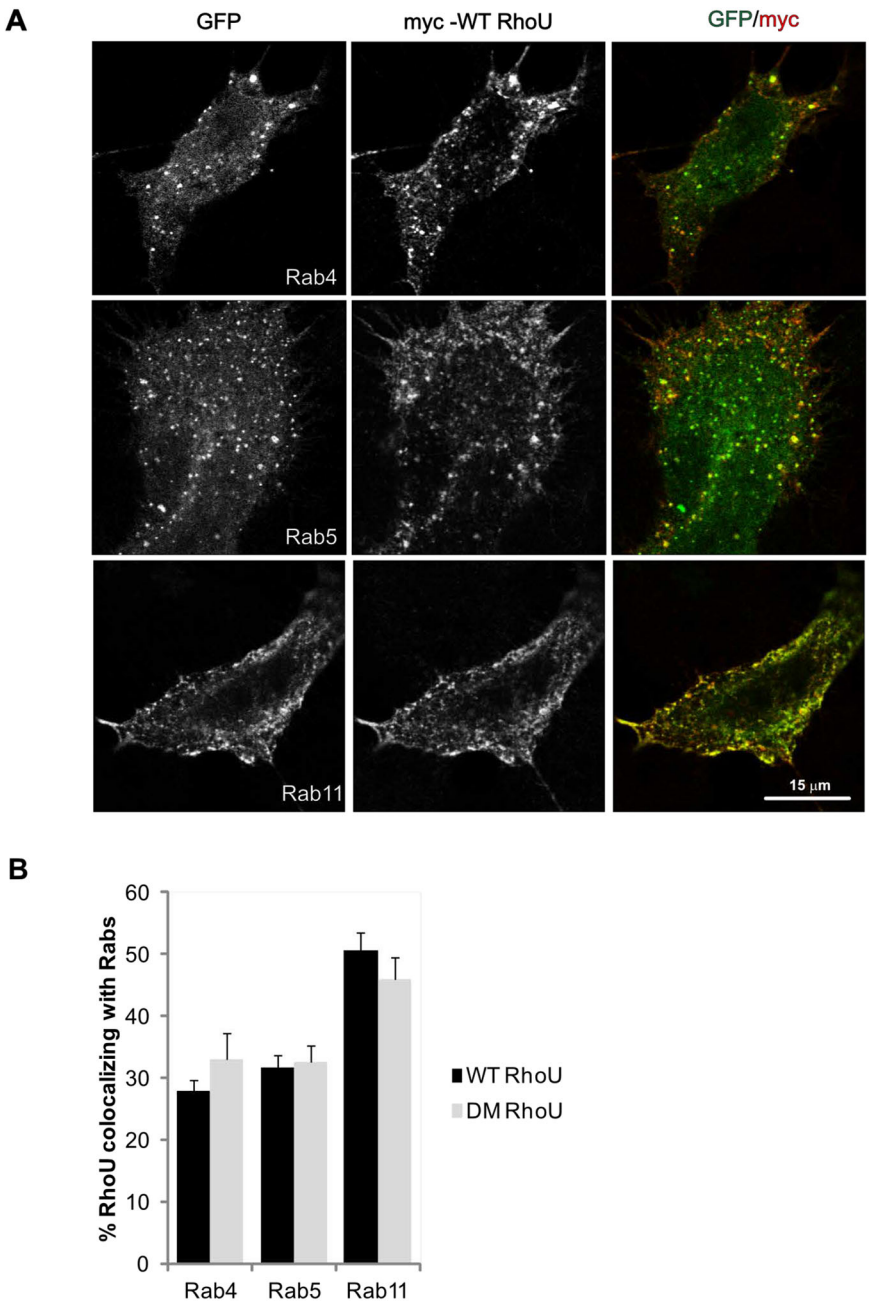

Fig. 6. RhoU is distributed all along the endocytic route. (A) Confocal microscopy analysis of HeLa cells co-expressing GFP–Rab4a, GFP–Rab5a or GFP–Rab11a and myc-tagged WT RhoU. (B) Quantification of RhoU colocalizing with Rab proteins. HeLa cells were transfected with GFP–Rab proteins along with myc–WT RhoU or myc DM–RhoU and the percentage colocalization determined. Data are mean±s.e.m. percentage colocalization (n=2 experiments, 15 cells per experiment).

ITSN2 partially colocalizes with RhoU on the Rab4 compartment

Because delays in Tf recycling occurred early after the pulse, we sought for colocalization of transfected myc–RhoU and HA–ITSN2 (S and L forms) with GFP–Rab4a, a marker of fast recycling endosomes (Grant and Donaldson, 2009). Although the degree of colocalization between HA–ITSN2, myc–RhoU and GFP–Rab4a was low, we could find a few vesicular structures containing RhoU and Rab4a with discrete amounts of ITSN2-L (Fig. 7A) or ITSN2-S (Fig. 7B). This suggests that ITSN2 could transiently associate with early endosomes that may contain Rab4a and RhoU (Sönnichsen et al., 2000; Zhang et al., 2011). To further confirm that ITSN2 could associate with early and/or sorting endosomes, we used spinning disk confocal microscopy to perform live-cell imaging of HeLa cells co-transfected with GFP–ITSN2-S and tagRFP-T–EEA1, a fluorescent tagged EEA1 that colocalizes with the endogenous proteins (Kalaidzidis et al., 2015; Navaroli et al., 2012). This revealed that there were in fact vesicles containing both EEA1 and ITSN2 (Fig. 8A). These vesicles are motile and can move toward an immobile EEA1-containing vesicle. Once in close contact, both types of vesicle remained associated for roughly 1 min before eventually segregating into two distinct vesicles, one containing both EEA1 and GFP–ITSN2-S and another one containing only EEA1 (Fig. 8A,B). Interestingly, vesicle motility analysis indicated that a fraction of EEA1 and ITSN2 vesicles were motile (Fig. 8C) and they can associate for a short period of time (Fig. 8D). Indeed, live-cell colocalization analysis showed that 15% of total vesicles were double stained for EEA1 and ITSN2 for less than 20 s. To substantiate our immunofluorescence data about partial colocalization of RhoU and ITSN2-S on a subset of vesicles, we co-transfected mCherry-tagged RhoU and GFP-tagged ITSN2-S in HeLa cells and fed them for 5 min with Tf–A647. In agreement with immunofluorescence colocalization data from fixed cells, live-cell

Journal of Cell Science (2020) 133, jcs234104. doi:10.1242/jcs.234104

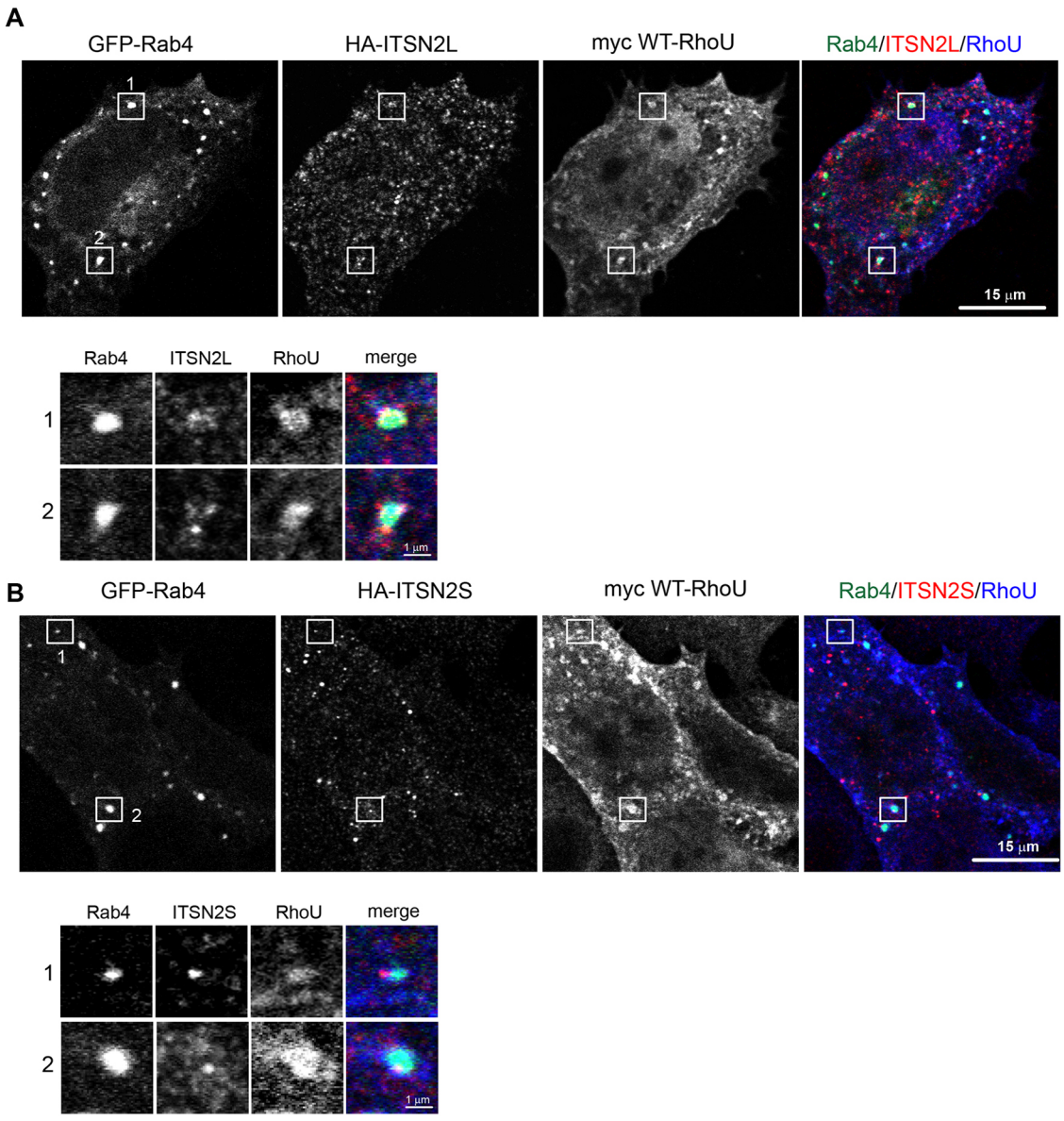

Fig. 7. ITSN2 and RhoU colocalize with Rab4-positive endosomes. (A) Confocal microscopy analysis of HeLa cells transfected with GFP–Rab4, HA–ITSN2-L and myc–WT RhoU. Boxes show regions magnified in inset 1 and 2. (B) Confocal microscopy analysis of HeLa cells transfected with GFP–Rab4, HA–ITSN2-S and myc–WT RhoU. Boxes show regions magnified in inset 1 and 2.

imaging using spinning disk confocal microscopy revealed that a subset of moving vesicles contained mCherry–RhoU, GFP–ITSN2-S and Tf–A647 (Fig. 8E). Vesicles with mCherry–RhoU and GFP–ITSN2-S were weakly stained for Tf–A647 (Fig. 8E, arrowheads) before fusion with mCherry–RhoU vesicles loaded with Tf. The association remained for ∼40 s before dissociation. These observations further strengthen the idea that RhoU and ITSN2-S are distributed on a subset of vesicles that transiently associate to potentially regulate the fate of cargo.

DISCUSSION

RhoU is an atypical Rho GTPase mostly involved in the regulation of cell migration and transformation (Berzat et al., 2005; Brady et al., 2009; Brazier et al., 2009; Chuang et al., 2007; Fort et al., 2011; Ory et al., 2007; Zhang et al., 2011). RhoU has been localized to diverse subcellular compartments including focal adhesions, the plasma membrane and intracellular vesicles. Although RhoU associates with endosomal compartments (Alan et al., 2010; Shutes et al., 2004; Zhang et al., 2011), no studies have addressed the potential function of RhoU in vesicle trafficking. Here, by looking for new RhoU binding partners and further characterizing the subcellular distribution of RhoU along the endocytic route, we provide evidence that RhoU binding to ITSN2 might regulate fast recycling of endocytosed cargo. Indeed, we identified ITSNs as part of a RhoU complex and showed that the second PxxPxR motif of RhoU acts as the preferential docking interface between RhoU and SH3 domains of ITSNs. Moreover, we found that silencing of ITSN2 but not ITSN1 reduced Tf recycling, leading to a global increase in Tf uptake. Interestingly, the defect in Tf recycling was phenocopied by RhoU silencing indicating that they act in the same pathway. Uptake of transferrin following a short pulse revealed that RhoU and ITSN2 are required for fast recycling of Tf. Importantly, defects in endocytosis and/or recycling observed in RhoU-silenced cells were restored by WT RhoU but not by a PxxP RhoU mutant,

Journal of Cell Science (2020) 133, jcs234104. doi:10.1242/jcs.234104

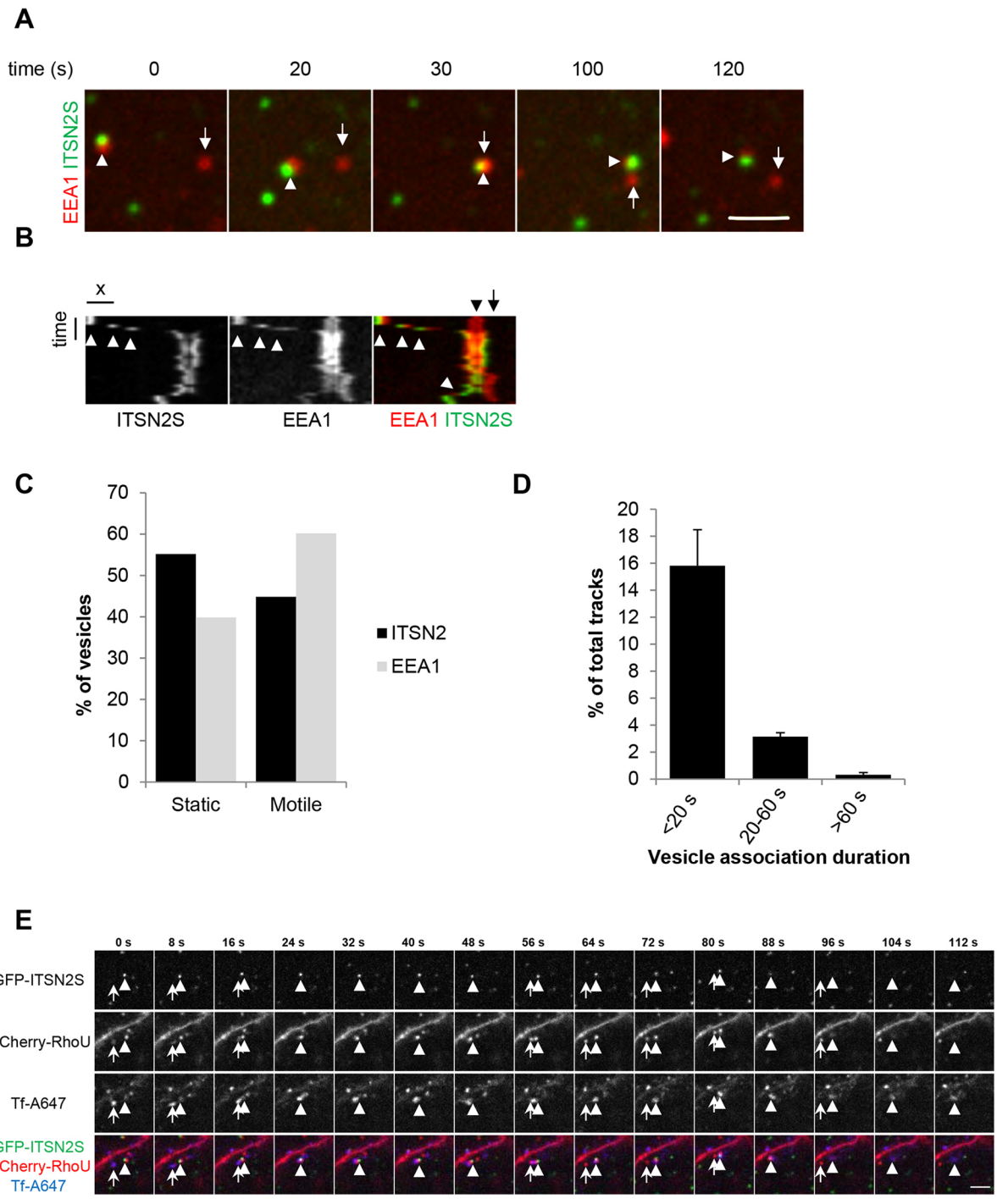

Fig. 8. ITSN2-S is transported with EEA1-positive endosomes. (A) Still images of HeLa cells co-transfected with GFP–ITSN2-S and TagRFP-T–EEA1. Cells were imaged using a spinning-disk confocal microscope for 2 min at 0.5 Hz. Arrowhead points to an endosome containing both ITSN2-S and EEA1. Arrow points to a single-stained EEA1-positive endosome. (B) Kymograph of the sequence. White arrowheads point to an endosome co-stained with ITSN2-S and EEA1 and the black arrowhead points to a single-stained EEA1 endosome. The double-stained endosome moves toward the EEA1-positive endosome and eventually segregates (white arrowhead, double-stained endosome; black arrow, EEA1-positive only endosome). (C) Quantification of static and motile vesicles from the movie. A total of 144 ITSN2- and 107 EEA1-positive vesicles were detected. Vesicles with displacement below 0.7 µm were considered static. (D) Quantification of ITSN2- and EEA1-positive vesicles that remained associated over time. ITSN2- and EEA1-positive vesicles were tracked over time and considered associated if tracks of vesicle centroids were separated by three pixels or fewer. Associations lasting less than 6 s (3 consecutive images) were discarded for the analysis. Tracks corresponding to double-stained vesicles were counted and normalized to the total number of tracks (sum of ITSN2- and EEA1-positive tracks) and expressed as mean±s.e.m. percentage (n=4 cells). (E) Images of HeLa cells co-transfected with GFP–ITSN2-S and mCherry–RhoU. Cells were incubated with 40 µg/ml Tf–A647 and imaged using a spinning-disk confocal microscope for 2 min at 1 Hz. Arrowhead points to a vesicle containing GFP–ITSN2-S, mCherry–RhoU and Tf–A647 after 10 min endocytosis. At t=0 s, the vesicle contained low amounts of Tf and then fused with an mCherry–RhoU-positive vesicle loaded with Tf–A647 (arrows, t=24 s). An mCherry–RhoU-positive vesicle subsequently split, with no associated Tf–A647 (arrow, t=56 s), then fused again (t=88 s). Finally, the GFP–ITSN2-S and mCherry–RhoU signals dissociate from the vesicle and only a vesicle with low amounts of Tf remained (arrowhead, t=96 s). Scale bars: A, 4 µm; B, 2 µm, 30 s; E, 4 µm.

Journal of Cell Science (2020) 133, jcs234104. doi:10.1242/jcs.234104

indicating that RhoU binding partners and potentially ITSN2 are linked to RhoU function in vesicle trafficking. Concomitantly, immunofluorescence analysis of ITSN2 and RhoU indicated that both proteins partially colocalized with Rab4, a marker of fast recycling vesicles. Finally, live-cell imaging showed that RhoU, ITSN2 and Tf partially and transiently colocalized. We therefore propose that interaction between RhoU and ITSN2 may occur on a subset of vesicles to drive fast recycling of cargos.

Due to their association with key components of clathrin-mediated endocytosis, including dynamin, synaptojanin and the AP2 complex (Praefcke et al., 2004; Yamabhai et al., 1998), most studies addressing ITSN1 and ITSN2 function have focused on the early phase of endocytosis. ITSN1 and ITSN2 are needed to progress from the formation of an early nucleation module to the clathrin-coated pit (CCP) by bridging FCHo and AP2 (Henne et al., 2010; Praefcke et al., 2004). In contrast to our expectations, the silencing of ITSN1 or ITSN2 did not inhibit Tf endocytosis, but instead either increased Tf accumulation in cells silenced for ITSN2 or had no effect in the case of ITSN1 silencing. Although surprising, our results are nonetheless consistent with previous reports showing that silencing of ITSNs has limited effect on Tf endocytosis (Das et al., 2007; Martin et al., 2006; Russo and O'Bryan, 2012; Yang et al., 2015) and with the idea that ITSN1 and ITSN2 can compensate each other in the early phase of clathrin-coated pit assembly (Henne et al., 2010). The fact that Tf accumulation was maximal after a short pulse of Tf uptake in the absence of RhoU or ITSN2 indicated that recycling defects occurred shortly after completion of CCP assembly. Accordingly, we detected accumulation of Tf in EEA1-positive endosomes, which constitute the main sorting platform of endocytosed cargos. We can nonetheless not fully exclude that Tf accumulation in EEA1-positive endosomes could be the result of accelerated Tf endocytosis, because we detected an increase in Tf uptake at an early endocytic phase, before recycling could take place. Interestingly, although EGF endocytosis is mediated by clathrin, silencing of RhoU or ITSN2 differentially regulated it. Although surprising at first glance, these data are in line with the unexpected low correlation between genes regulating Tf and EGF endocytosis (Collinet et al., 2010).

Endosomes can be seen as a dynamic arrangement of membrane domains containing various amounts of Rab proteins that regulate the fate of vesicle (Rink et al., 2005; Sönnichsen et al., 2000), and our colocalization analysis revealed that RhoU colocalized with Rab5, Rab4 and Rab11 but much less with Rab7, indicating that RhoU is most likely involved in recycling of cargo rather than its degradation. The prominent colocalization of RhoU with Rab11 is, however, intriguing because no defect in slow recycling was noticed. One possible explanation is that overexpression of Rab proteins might affect the proportion of the different endocytic vesicle pools, each in different ways. In that context, it is difficult to compare colocalization levels when Rab proteins are overexpressed.

Because RhoU colocalized with ITSN2 on a subset of Rab4-containing vesicles, a marker of fast vesicle recycling, it suggests that the RhoU–ITSN2 interaction might constitute a molecular switch to drive fast recycling of vesicular cargos. The use of fluorescent Tf as a readout of endocytosis does not exclude that other cargo, including receptors or adhesion molecules, might be regulated by the RhoU–ITSN2 interaction. Indeed, despite various modes of entry, cargos eventually meet in EEA1-positive endosomes, from where they are recycled back to the plasma membrane or degraded (Barysch et al., 2009; Lakadamyali et al., 2006; Leonard et al., 2008). Interestingly, RhoU has been implicated in several biological processes that might depend on plasma membrane protein recycling, for example, cell migration (Chuang et al., 2007; Fort et al., 2011; Ory et al., 2007) and cell polarity (Brady et al., 2009). Whether RhoU and ITSN2 control cell adhesion molecule turnover has to be investigated, but Rab4-dependent recycling of integrins at the plasma membrane is key to cell motility and cell adhesion turnover (Arjonen et al., 2012; Roberts et al., 2001), and both RhoU and ITSN2 silencing alters cell–cell junction and epithelial cyst formation in a three-dimensional matrix (Brady et al., 2009; Qin et al., 2010). RhoU has also been linked to EGFR signaling thanks to Grb2 binding. Upon EGF stimulation, endosomal RhoU is recruited by Grb2 in the EGFR complex to sustain JNK activation. Grb2 binds to RhoU through the same motif as ITSN2 (Zhang et al., 2011). Whether ITSN2 and Grb2 compete for RhoU binding and modulate EGFR signaling would be an interesting issue to address, especially because ITSN2 is phosphorylated in response to EGF in an endocytosis-dependent manner (Novokhatska et al., 2013). Finally, RhoU expression levels are regulated by various signals including Wnt-1, RANKL (also known as TNFSF11) and Notch to induce cell differentiation (Bhavsar et al., 2012; Brazier et al., 2006; Schiavone et al., 2009; Tao et al., 2001). Therefore, according to its expression levels, RhoU might modulate the rate of endocytosis and/or recycling of receptors to control signal output and cell fate.

The subcellular localization analysis of RhoU and ITSN2 indicated that both proteins are mutually excluded from plasma membrane compartments where RhoU or ITSN2 accumulates. RhoU is found in focal adhesions but not in CCP where ITSN2 is enriched. Conversely, ITSN2 is not localized to focal adhesions, indicating that RhoU and ITSN2 might achieve distinct functions and meet on endosomes to ensure specific cargo recycling. Vesicular localization of ITSNs also suggests that, in addition to their role in CCP maturation, they might have a function in vesicle trafficking. Indeed, a few reports suggest that ITSNs might regulate endosomal trafficking. For example, yeast two-hybrid screens have identified Rabaptin-5 (also known as RABEP1) and the kinesin KIF16B as potential binding partners of ITSN1 and ITSN2 (Wong et al., 2012; Yang et al., 2015). Both Rabaptin-5 and KIF16B coordinate Rab5 and Rab4 for efficient vesicle recycling (Hoepfner et al., 2005; Pagano et al., 2004; Stenmark et al., 1995). Recently, ITSN1-S has been reported to localize to Rab4-positive vesicles (Gryaznova et al., 2018) and to interact with DENND2B, an exchange factor for Rab13 involved in EGF receptor recycling (Ioannou et al., 2017). ITSN1-knockout mice show only minor (Yu et al., 2008) or no defects (Sakaba et al., 2013) in CME-dependent synaptic vesicle recycling in neurons, but neurons have enlarged EEA1-containing endosomes (Yu et al., 2008). Together with our data showing that ITSN2 localizes to Rab4, associates with EEA1-containing moving vesicles and transiently colocalizes with RhoU and Tf in living cells, this provides clues for potential roles of ITSNs in vesicle transport and recycling. The fact that ITSN1 and ITSN2 silencing had different consequences for Tf recycling suggests that, although they can compensate each other in CCP maturation, they might have distinct functions in vesicular trafficking.

Our findings question whether RhoU activity might be regulated by ITSNs and/or RhoU might modulate Cdc42 activity. RhoU is believed to be constitutively active because its GDP/GTP exchange rate *in vitro* is spontaneous and fast. However, deletion of the RhoU N terminus containing the PxxP motifs enhances the ability of the protein to bind and activate PAK to promote cell transformation, suggesting that the RhoU N terminus negatively regulates RhoU activity (Shutes et al., 2004). Modulation of RhoU activity has been proposed to occur in response to EGF signaling, in which binding of Grb2 to RhoU might relieve N-terminus-dependent inhibition (Zhang et al., 2011). Therefore, the binding of ITSNs to RhoU

Journal of Cell Science (2020) 133, jcs234104. doi:10.1242/jcs.234104

might be a way to locally enhance RhoU activity. Further work will be needed to develop tools able to monitor local RhoU activities. Remarkably, by testing individual SH3 domains, we found that three domains of ITSN1 (SH3A, -C, -E) and only one domain of ITSN2 (SH3E) mediated RhoU binding. This discrimination is rather surprising considering that SH3A, -C and -E domains of ITSNs fall into canonical classes of SH3 domains and preferentially bind to classII PxxPxR motifs (Teyra et al., 2017). Our *in vitro* experiments show that the M2 domain is critical, whereas the M1 domain contributes moderately to SH3 binding suggesting that M1 and amino acids between M1 and M2 might constitute an extended surface to promote selective binding of RhoU to SH3 domains (Gorelik and Davidson, 2012). It also suggests that, depending on the ITSN engaged with RhoU, the stoichiometry of the ITSN–RhoU complex might be different.

Finally, ITSNs are well known exchange factors for Cdc42 thanks to their Dbl homology (DH) domain. The long form of ITSNs is less potent to activate Cdc42 than the DH domain alone, suggesting that SH3 domains of ITSN negatively regulate DH-dependent nucleotide-exchange activity (Zamanian and Kelly, 2003). RhoU binding to ITSNs might therefore relieve auto-inhibition and facilitate local Cdc42 activation. Activated Cdc42 controls filopodia formation and cell polarity, two features also controlled by RhoU (Alan et al., 2010; Brady et al., 2009; Ruusala and Aspenström, 2008). By binding to WASP proteins, ITSN2-L facilitates Cdc42-dependent actin polymerization (Klein et al., 2009; McGavin et al., 2001). Actin polymerization might act as a scaffold to limit cargo diffusion on endosomes and control their fate (Simonetti and Cullen, 2019). In contrast to Cdc42, RhoU does not interact with the GTPase-binding domain of WASP (Saras et al., 2004), and among RhoU effectors, none has been reported to mediate actin polymerization. Our study therefore raises new issues surrounding a potential crosstalk between RhoU, ITSN2 and Cdc42 to regulate sorting of cargos.

MATERIALS AND METHODS

Constructs and antibodies

Human RhoU was PCR amplified as a BamHI/EcoRI fragment from pRK5-myc RhoU constructs (a kind gift from Dr Pontus Aspenström, IGP, Uppsala, Sweden) and subcloned into pGEX-4T1 (GE Healthcare, USA) between the BamHI/EcoRI sites. The constructs encoding mCherry-RhoU were generated by digesting pGEX-4T1-RhoU with BamHI and PstI and subcloning the insert into pmCherry-C1 (TaKara Bio, USA) between BglII/PstI sites.

The constructs encoding the myc-tagged mouse RhoU (WT or proline to alanine mutants) were a kind gift from Dr Daniel Billadeau (Mayo Clinic, Rochester, MN, USA) and were described previously (Zhang et al., 2011). For lentiviruses production, mouse RhoU was cloned into pLenti-EF1α-WPRE vector [previously described in Rossolillo et al. (2012)] between NdeI and SalI sites (generated by Dr Paola Rossolillo, IGBMC, Strasbourg, France).

The constructs encoding SH3 domains of ITSN1 or ITSN2 fused to GST and Omni-tagged ITSN1-L were as described previously (Gryaznova et al., 2015; Tsyba et al., 2008). The cDNAs encoding human ITSN2-S were a kind gift from Dr Susana de la Luna (CRG, Barcelona, Spain). The full coding sequence of ITSN2-S was subcloned into the BamHI site of the pEGFP-C1 plasmid (TaKara Bio, USA). The plasmids encoding GFP-tagged human Rab proteins (Rab4a, Rab5a, Rab11a, Rab7a) were a kind gift from Dr Philippe Chavrier (Institut Curie, Paris, France).

The rabbit polyclonal anti-EEA1 was purchased from Santa Cruz Biotechnology (Heidelberg, Germany; #N-19; 1:200), the monoclonal anti-myc (clone 4A6; 1:200, or 1:100 for Alexa-555 conjugated) and the polyclonal anti-RhoU (#ABS-99; 1:1000) antibodies were from Millipore (Saint Quentin Fallavier, France), the polyclonal anti-ITSN2 antibody was from Novus Biologicals (Lille, France; #NBP1-71833; 1:2000), the polyclonal anti-Rab11 antibody was from Thermo Fisher Scientific (Courtaboeuf, France; #715300; 1:50). Unlabeled and fluorescent transferrin were from Sigma (Saint Quentin Fallavier, France). Mouse polyclonal rabbit α-Omni (M-19; 1:1000) antibodies were from Santa Cruz Biotechnology. Rabbit polyclonal α-GST antibodies were from Sigma (#G1160; 1:1000).

Cell culture and transfection

HEK293T and HeLa (kind gift from Dr Fabien Alpy, IGBMC, Strasbourg) cells were cultured in Dulbecco's modified Eagle's medium (DMEM) supplemented with 10% fetal bovine serum at 37°C in 5% CO_2. Plasmid DNA was transfected, according to manufacturer's instructions, using jetPEI™ (Polyplus, Illkirch, France).

For siRNA transfection, 2×10^4 HeLa cells/cm^2 were seeded 24 h prior to siRNA transfection. Lipofectamine RNAiMax (Thermo Fisher Scientific, Courtaboeuf, France) and 50 nM of a mix of four siRNAs directed against *ITSN1, ITSN2, CLTC or RhoU* (On Target Plus Smart Pool siRNA; Dharmacon, Cambridge, UK) were used (see Table S1 for sequences). Cells were cultured for 48 h before experiments, and silencing was estimated and normalized to actin contents using western blotting. We obtained more than 70% silencing for each protein in each experiment.

Generation of stable lines expressing mouse RhoU

Lentiviral vectors were produced as previously described (Naldini et al., 1996) and generated by Dr Paola Rossolillo (IGBMC, Strasbourg, France). Briefly, HEK293T were co-transfected with pCMVΔR8.91-based plasmids, pHCMV-G plasmids encoding the VSV-G envelope protein, and pLenti-EF1α-myc-RhoU (WT or DM) using the polyethylenimine method and following the manufacturer's instructions (PEI, MW 25000, linear; Polysciences, Warrington, PA, USA). The medium was replaced 6 h after transfection and, 72 h later, the virus-containing supernatant was collected, filtered through a 0.45 µm filter and concentrated 40-fold in Vivaspin 20 columns (MW cutoff 50 kDa; Sartorius Stedim Biotech). 10^4 HeLa cells/cm^2 were seeded 24 h prior to infection with lentivirus (1:1500) for 4 h. 24 h after infection, puromycin (2 µg/ml) was added to select cells for heterologous sequence integration. Once selection was achieved, cells were split and seeded at low density (12 cells/cm^2) to isolate single colonies. After amplification, clones were tested using western blotting and immunofluorescence for myc–RhoU expression and subcellular localization, respectively.

GST pulldown and co-immunoprecipitation assays

GST fusion proteins were produced in *Escherichia coli* BL21 cells. After isopropylthiogalactoside (IPTG) induction, pellets of bacteria were resuspended in lysis buffer containing 50 mM Tris-HCl (pH 8), 2 mM $MgCl_2$, 0.2 mM $Na_2S_2O_5$, 10% glycerol, 20% sucrose, 2 mM dithiothreitol, protease inhibitor cocktail (Roche, Mannheim, Germany) and then sonicated. Cell lysates were centrifuged for 20 min at 4°C at 45,000 ***g*** and the supernatants were incubated with glutathione-coupled Sepharose 4B beads (Sigma) for 30 min at 4°C. After three washes with lysis buffer, amounts of GST fusion proteins bound to the beads were estimated using Coomassie-stained SDS gels.

HEK293T cells transfected with myc-tagged RhoU (WT or proline mutants) were rapidly washed in ice-cold PBS and lysed on ice with 20 mM Tris-HCl (pH 8), 2 mM $MgCl_2$, 1% IGEPAL CA-630, 10 µM GDP, 150 mM NaCl and protease inhibitor cocktail. Lysates were cleared for 5 min at 17,000 ***g*** at 4°C and aliquots were taken from the supernatant to determine the protein concentration in the total cell lysate. 20 µg of bacterially produced SH3 domains of ITSN1 or ITSN2 fused to the GST protein and bound to glutathione-coupled Sepharose beads were added to cell lysates and maintained for 2 h at 4°C. Beads with bound proteins were washed four times in wash buffer (20 mM Tris-HCl, pH 8, 150 mM NaCl, 0.1% IGEPAL CA-630, 2 mM $MgCl_2$, 10 µM GDP), eluted in Laemmli sample buffer and then analyzed by western blotting for precipitated RhoU.

For immunoprecipitations, HEK293T cells were lysed in IP buffer [150 mM NaCl, 20 mM Tris-HCl, pH 7.5, 10% glycerol, 0.5% NP40, 5 mM $MgCl_2$ and protease inhibitor cocktail (Sigma)] and centrifuged for 15 min at 16,000 ***g***. Supernatant (2 mg of protein) was incubated with 2 µg of target antibodies and 20 µl of Protein A/G Plus Ultralink Resin (ThermoScientific) for 4 h at 4°C.

Journal of Cell Science (2020) 133, jcs234104. doi:10.1242/jcs.234104

Then beads were washed four times with IP buffer. Immunoprecipitated complexes were eluted with Laemmli buffer and analyzed by western blotting.

Endocytosis, recycling assays and immunofluorescence

For continuous endocytosis assays, HeLa cells were serum starved for 30 min in DMEM supplemented with 0.5% BSA (DMEM/BSA) and incubated for 15 min with DMEM/BSA containing 10 µg/ml Alexa-647-conjugated transferrin (Thermo Fisher Scientific) at 37°C. For EGF endocytosis assay, cells were serum starved overnight and incubated for 15 min with 2 ng/ml TRITC-conjugated epidermal growth factor (EGF, Thermo Fisher Scientific). Cells were transferred on ice and washed twice with ice-cold PBS before fixation for 10 min with 4% (w/v) paraformaldehyde in PBS. Nuclei were stained with Hoechst.

For fast recycling assays, HeLa cells were serum starved for 30 min in DMEM supplemented with 0.5% BSA (DMEM/BSA) and incubated on ice for 1 h with DMEM/BSA containing 20 µg/ml Alexa-647-conjugated transferrin. Cells were incubated for 2 min in DMEM/BSA at 37°C and transferred back on ice. Transferrin at the cell surface was removed by incubating cells for 3 min in ice-cold stripping buffer (0.1 M glycine, 150 mM NaCl, pH 3.0), washed twice with ice-cold DMEM/BSA and incubated for the indicated times at 37°C in DMEM/BSA supplemented with 500 µg/ml unlabeled transferrin. Cells were fixed for 10 min with 4% (w/v) paraformaldehyde in PBS. For EEA1 staining, cells were permeabilized for 5 min with 0.1% Triton X-100 (v/v) in PBS and incubated with polyclonal anti-EEA1 antibodies diluted with 3% BSA (w/v) in PBS for 45 min at room temperature. For Rab11 staining, cells were incubated for 45 min with anti-Rab11 antibodies diluted with 0.2% saponin (w/v) and 1% BSA in PBS. After three washes in PBS, primary antibodies were detected using the relevant Alexa-Fluor-conjugated secondary antibodies. Cells were mounted in Mowiol 40-88 (Sigma) and observed under a TCS SP5 confocal microscope (Leica Microsystems, Nanterre, France) using a 63× objective (NA 1.40).

Image analysis

In order to quantify Tf uptake, a stack of three planes with large field of view (1024×1024 at 700 Hz, 91 nm pixel size, 500 nm z step) was taken by confocal microscopy to include several cells in one field and to select the best equatorial plane. Images were analyzed using open source Icy software (de Chaumont et al., 2012; http://icy.bioimageanalysis.org/) and protocol (NewColocalizer_with_binary_and_excel_output_v1_batch; available on the Icy website). Each cell was manually delineated using phase contrast images and vesicles were segmented using wavelet spot detection (Olivo-Marin, 2002). Segmented objects were considered colocalized if the distances between their centroids were below four pixels, and were expressed as a percentage. To estimate the relative amount of Tf in EEA1 or Rab11 compartments, integrated Tf–A647 fluorescence in objects resulting from the segmentation of each compartment was measured and normalized to the total amount of Tf–A647 measured in the cell.

Flow cytometry analysis

HeLa cells were serum starved for 30 min with DMEM/BSA at 37°C and incubated for 15 min with 10 µg/ml fluorescent transferrin in DMEM/BSA. Cells were transferred on ice, lifted by gentle scraping in PBS containing 0.5 mM EDTA, resuspended and incubated with propidium iodide to exclude dead cells prior to analysis using a Macsquant analyzer (Miltenyi biotec, Bergisch Gladbach, Germany). For kinetics analysis of transferrin recycling, cells were incubated for 1 h at 4°C with 20 µg/ml of fluorescent transferrin following serum starvation. Cells were washed with ice-cold Hank's Balanced Salt Solution (HBSS) and either analyzed by flow cytometry to evaluate transferrin binding to the cell surface or incubated for the indicated amount of time at 37°C before acid wash to remove remaining cell-surface transferrin. At least 10,000 cells were analyzed and the mean fluorescence intensity of each condition was normalized to the mean fluorescence intensity of the control cells for comparison. For the transferrin recycling assay, HeLa cells were incubated for 30 min at 37°C after 30 min starvation. Membrane-bound transferrin was stripped away by incubating cells in ice-cold stripping buffer for 3 min. Cells were incubated for the indicated amount of time before analysis using flow cytometry. For fast recycling analysis, cells were maintained for 1 h on ice with 10 µg/ml fluorescent transferrin in DMEM/BSA. Cells were quickly washed and transferred to 37°C for 2 min before stripping away plasma membrane-bound transferrin. Cells were either immediately analyzed using flow cytometry or incubated for the indicated amount of time before analysis. Transferrin recycling was estimated as: $\frac{(F_0 - F_t)}{F_0} \times 100$, where F_0 and F_t are the transferrin mean fluorescence after stripping and after incubation at 37°C, respectively.

Western blotting

Cells were washed twice with ice cold PBS and lysed in RIPA buffer (20 mM Tris-HC,l pH 7.4, 137 mM NaCl, 10% glycerol, 1% Triton X-100, 0.1% SDS, 0.5% sodium deoxycholate and 1 mM EDTA) for 20 min on ice. Lysates were centrifuged for 10 min at 20,000 ***g***, and protein concentration determined using a BioRad protein assay. 20 µg of proteins were separated on a Novex 4–12% Bis-Tris gel (Thermo Fisher Scientific) and transferred to nitrocellulose membrane. Blots were blocked for 1 h at room temperature in Tris-buffered saline containing 3% BSA and 0.1% Tween-20, and incubated overnight with the indicated primary antibodies. After three washes, blots were incubated with secondary antibodies coupled to HRP. Detection was carried out with Super Signal West Dura Extended Duration substrate (Thermo Fisher Scientific) and immunoreactive bands were imaged using a Chemismart 5000 (Vilber Lourmat, Marne-la-Vallée, France).

Time-lapse video microscopy

HeLa cells were transfected with GFP–ITSN2-S and TagRFP-T–EEA1 (Addgene #42635), or with GFP–ITSN2-S and mCherry–RhoU, and observed under a spinning disk microscope (Zeiss Axio Observer Z1 with a Yokogawa CSU X1 confocal head) at 37°C using a 63×1.4 NA objective. Images of each fluorescent protein were sequentially acquired to avoid bleed-through using 488 nm and 561 nm laser lines at 0.5 Hz. BP525/50 and BP629/62 emission filters were used to retrieve GFP–ITSN2-S and TagRFP–EEA1 signals, respectively. For simultaneous imaging of Tf–A647, the 633 nm laser line and a quadriband filter was used. The acquisition sequence was driven by Metamorph software (Molecular devices, San Jose, CA, USA). Movies were opened in Icy software, single-spot detected for each channel and analyzed using the Track Manager plugin. The track processor for interaction analysis was used to estimate vesicle association duration. Vesicles were considered associated if they were separated by less than three pixels. Only vesicles that remained associated for more than three consecutive frames (6 s) were considered for analysis.

Statistical analysis

Statistical analyses were performed using SigmaPlot 11.0 (Ritme, Paris, France). One-way ANOVA followed by Holm–Sidak post hoc test was performed to assess the difference between groups when data followed normal distribution and equal variance. If the normality test failed, significance was estimated using the non-parametric Kruskal–Wallis test followed by Dunn's post-hoc test.

Acknowledgements

We acknowledge the generosity of Dr Susana de la Luna (CRG, Barcelona, Spain), Dr Daniel Billadeau (Mayo Clinic, Rochester, MN, USA) and Dr Philippe Chavrier for kindly providing us with human ITSN2, mouse RhoU and human Rabs coding plasmids, respectively. We acknowledge the confocal microscopy facilities of Plateforme Imagerie In Vitro, the cytometry facility at INCI and Dr Jean-Daniel Fauny (IBMC, UPR3512, Strasbourg) for technical assistance with spinning disk confocal microscopy. We acknowledge Dr Paola Rossolillo (IGBMC, Illkirch, France) for generating pLenti-EF1α-myc-RhoU plasmids and lentiviruses.

Competing interests

The authors declare no competing or financial interests.

Author contributions

Conceptualization: O.G., S.O.; Methodology: O.G., P.C.; Investigation: O.G., P.C., S.K., T.G., S.O.; Resources: A.B.; Writing - original draft: S.O.; Writing - review & editing: O.G., P.T., A.B., N.V., A.R., S.G.; Supervision: S.G., S.O.; Project administration: S.G., S.O.

Funding
This work was supported by Centre National de la Recherche Scientifique institutional funding.

Supplementary information
Supplementary information available online at
https://jcs.biologists.org/lookup/doi/10.1242/jcs.234104.supplemental

References

Aguet, F., Antonescu, C. N., Mettlen, M., Schmid, S. L. and Danuser, G. (2013). Advances in analysis of low signal-to-noise images link dynamin and AP2 to the functions of an endocytic checkpoint. *Dev. Cell* **26**, 279-291. doi:10.1016/j.devcel.2013.06.019

Alan, J. K., Berzat, A. C., Dewar, B. J., Graves, L. M. and Cox, A. D. (2010). Regulation of the Rho family small GTPase Wrch-1/RhoU by C-terminal tyrosine phosphorylation requires src. *Mol. Cell. Biol.* **30**, 4324-4338. doi:10.1128/MCB.01646-09

Arjonen, A., Alanko, J., Veltel, S. and Ivaska, J. (2012). Distinct recycling of active and inactive β1 integrins. *Traffic* **13**, 610-625. doi:10.1111/j.1600-0854.2012.01327.x

Aspenström, P., Ruusala, A. and Pacholsky, D. (2007). Taking Rho GTPases to the next level: the cellular functions of atypical Rho GTPases. *Exp. Cell Res.* **313**, 3673-3679. doi:10.1016/j.yexcr.2007.07.022

Barysch, S. V., Aggarwal, S., Jahn, R. and Rizzoli, S. O. (2009). Sorting in early endosomes reveals connections to docking- and fusion-associated factors. *Proc. Natl. Acad. Sci. USA* **106**, 9697-9702. doi:10.1073/pnas.0901444106

Berzat, A. C., Buss, J. E., Chenette, E. J., Weinbaum, C. A., Shutes, A., Der, C. J., Minden, A. and Cox, A. D. (2005). Transforming activity of the Rho family GTPase, Wrch-1, a Wnt-regulated Cdc42 homolog, is dependent on a novel carboxyl-terminal palmitoylation motif. *J. Biol. Chem.* **280**, 33055-33065. doi:10.1074/jbc.M507362200

Bhavsar, P. J., Infante, E., Khwaja, A. and Ridley, A. J. (2012). Analysis of Rho GTPase expression in T-ALL identifies RhoU as a target for Notch involved in T-ALL cell migration. *Oncogene* **32**, 198-208. doi:10.1038/onc.2012.42

Brady, D. C., Alan, J. K., Madigan, J. P., Fanning, A. S. and Cox, A. D. (2009). The transforming Rho family GTPase Wrch-1 disrupts epithelial cell tight junctions and epithelial morphogenesis. *Mol. Cell. Biol.* **29**, 1035-1049. doi:10.1128/MCB.00336-08

Brazier, H., Stephens, S., Ory, S., Fort, P., Morrison, N. and Blangy, A. (2006). Expression profile of RhoGTPases and RhoGEFs during RANKL-stimulated osteoclastogenesis: identification of essential genes in osteoclasts. *J. Bone Miner. Res.* **21**, 1387-1398. doi:10.1359/jbmr.060613

Brazier, H., Pawlak, G., Vives, V. and Blangy, A. (2009). The Rho GTPase Wrch1 regulates osteoclast precursor adhesion and migration. *Int. J. Biochem. Cell Biol.* **41**, 1391-1401. doi:10.1016/j.biocel.2008.12.007

Chamberland, J. P., Antonow, L. T., Dias Santos, M. and Ritter, B. (2016). NECAP2 controls clathrin coat recruitment to early endosomes for fast endocytic recycling. *J. Cell Sci.* **129**, 2625-2637. doi:10.1242/jcs.173708

Chuang, Y., Valster, A., Coniglio, S. J., Backer, J. M. and Symons, M. (2007). The atypical Rho family GTPase Wrch-1 regulates focal adhesion formation and cell migration. *J. Cell Sci.* **120**, 1927-1934. doi:10.1242/jcs.03456

Ciechanover, A., Schwartz, A. L., Dautry-Varsat, A. and Lodish, H. F. (1983). Kinetics of internalization and recycling of transferrin and the transferrin receptor in a human hepatoma cell line. Effect of lysosomotropic agents. *J. Biol. Chem.* **258**, 9681-9689.

Collinet, C., Stöter, M., Bradshaw, C. R., Samusik, N., Rink, J. C., Kenski, D., Habermann, B., Buchholz, F., Henschel, R., Mueller, M. S. et al. (2010). Systems survey of endocytosis by multiparametric image analysis. *Nature* **464**, 243-249. doi:10.1038/nature08779

Das, M., Scappini, E., Martin, N. P., Wong, K. A., Dunn, S., Chen, Y.-J., Miller, S. L. H., Domin, J. and O'Bryan, J. P. (2007). Regulation of neuron survival through an intersectin-phosphoinositide 3'-kinase C2beta-AKT pathway. *Mol. Cell. Biol.* **27**, 7906-7917. doi:10.1128/MCB.01369-07

de Chaumont, F., Dallongeville, S., Chenouard, N., Hervé, N., Pop, S., Provoost, T., Meas-Yedid, V., Pankajakshan, P., Lecomte, T., Le Montagner, Y. et al. (2012). Icy: an open bioimage informatics platform for extended reproducible research. *Nat. Methods* **9**, 690-696. doi:10.1038/nmeth.2075

Fort, P., Guémar, L., Vignal, E., Morin, N., Notarnicola, C., Barbara, P. de S. and Faure, S. (2011). Activity of the RhoU/Wrch1 GTPase is critical for cranial neural crest cell migration. *Dev. Biol.* **350**, 451-463. doi:10.1016/j.ydbio.2010.12.011

Garrard, S. M., Capaldo, C. T., Gao, L., Rosen, M. K., Macara, I. G. and Tomchick, D. R. (2003). Structure of Cdc42 in a complex with the GTPase-binding domain of the cell polarity protein, Par6. *EMBO J.* **22**, 1125-1133. doi:10.1093/emboj/cdg110

Gorelik, M. and Davidson, A. R. (2012). Distinct peptide binding specificities of Src homology 3 (SH3) protein domains can be determined by modulation of local energetics across the binding interface. *J. Biol. Chem.* **287**, 9168-9177. doi:10.1074/jbc.M111.330753

Grant, B. D. and Donaldson, J. G. (2009). Pathways and mechanisms of endocytic recycling. *Nat. Rev. Mol. Cell Biol.* **10**, 597-608. doi:10.1038/nrm2755

Gryaznova, T., Kropyvko, S., Burdyniuk, M., Gubar, O., Kryklyva, V., Tsyba, L. and Rynditch, A. (2015). Intersectin adaptor proteins are associated with actin-regulating protein WIP in invadopodia. *Cell. Signal.* **27**, 1499-1508. doi:10.1016/j.cellsig.2015.03.006

Gryaznova, T., Gubar, O., Burdyniuk, M., Kropyvko, S. and Rynditch, A. (2018). WIP/ITSN1 complex is involved in cellular vesicle trafficking and formation of filopodia-like protrusions. *Gene* **674**, 49-56. doi:10.1016/j.gene.2018.06.078

Hao, M. and Maxfield, F. R. (2000). Characterization of rapid membrane internalization and recycling. *J. Biol. Chem.* **275**, 15279-15286. doi:10.1074/jbc.275.20.15279

Henne, W. M., Boucrot, E., Meinecke, M., Evergren, E., Vallis, Y., Mittal, R. and McMahon, H. T. (2010). FCHo proteins are nucleators of clathrin-mediated endocytosis. *Science* **328**, 1281-1284. doi:10.1126/science.1188462

Hoepfner, S., Severin, F., Cabezas, A., Habermann, B., Runge, A., Gillooly, D., Stenmark, H. and Zerial, M. (2005). Modulation of receptor recycling and degradation by the endosomal kinesin KIF16B. *Cell* **121**, 437-450. doi:10.1016/j.cell.2005.02.017

Ioannou, M. S., Kulasekaran, G., Fotouhi, M., Morein, J. J., Han, C., Tse, S., Nossova, N., Han, T., Mannard, E. and McPherson, P. S. (2017). Intersectin-s interaction with DENND2B facilitates recycling of epidermal growth factor receptor. *EMBO Rep.* **18**, 2119-2130. doi:10.15252/embr.201744034

Jaffe, A. B. and Hall, A. (2005). RHO GTPASES: biochemistry and biology. *Annu. Rev. Cell Dev. Biol.* **21**, 247-269. doi:10.1146/annurev.cellbio.21.020604.150721

Kalaidzidis, I., Miaczynska, M., Brewińska-Olchowik, M., Hupalowska, A., Ferguson, C., Parton, R. G., Kalaidzidis, Y. and Zerial, M. (2015). APPL endosomes are not obligatory endocytic intermediates but act as stable cargo-sorting compartments. *J. Cell Biol.* **211**, 123-144. doi:10.1083/jcb.201311117

Klein, I. K., Predescu, D. N., Sharma, T., Knezevic, I., Malik, A. B. and Predescu, S. (2009). Intersectin-2L regulates caveola endocytosis secondary to Cdc42-mediated actin polymerization. *J. Biol. Chem.* **284**, 25953-25961. doi:10.1074/jbc.M109.035071

Lakadamyali, M., Rust, M. J. and Zhuang, X. (2006). Ligands for clathrin-mediated endocytosis are differentially sorted into distinct populations of early endosomes. *Cell* **124**, 997-1009. doi:10.1016/j.cell.2005.12.038

Leonard, D., Hayakawa, A., Lawe, D., Lambright, D., Bellve, K. D., Standley, C., Lifshitz, L. M., Fogarty, K. E. and Corvera, S. (2008). Sorting of EGF and Transferrin at the plasma membrane and by cargo-specific signaling to EEA1-enriched endosomes. *J. Cell Sci.* **121**, 3445-3458. doi:10.1242/jcs.031484

Martin, N. P., Mohney, R. P., Dunn, S., Das, M., Scappini, E. and O'Bryan, J. P. (2006). Intersectin regulates epidermal growth factor receptor endocytosis, ubiquitylation, and signaling. *Mol. Pharmacol.* **70**, 1643-1653. doi:10.1124/mol.106.028274

McGavin, M. K. H., Badour, K., Hardy, L. A., Kubiseski, T. J., Zhang, J. and Siminovitch, K. A. (2001). The intersectin 2 adaptor links wiskott aldrich syndrome protein (WASp)-mediated actin polymerization to T cell antigen receptor endocytosis. *J. Exp. Med.* **194**, 1777-1787. doi:10.1084/jem.194.12.1777

Naldini, L., Blömer, U., Gallay, P., Ory, D., Mulligan, R., Gage, F. H., Verma, I. M. and Trono, D. (1996). In Vivo gene delivery and stable transduction of nondividing cells by a lentiviral vector. *Science* **272**, 263-267. doi:10.1126/science.272.5259.263

Navaroli, D. M., Bellvé, K. D., Standley, C., Lifshitz, L. M., Cardia, J., Lambright, D., Leonard, D., Fogarty, K. E. and Corvera, S. (2012). Rabenosyn-5 defines the fate of the transferrin receptor following clathrin-mediated endocytosis. *Proc. Natl. Acad. Sci. USA* **109**, E471-E480. doi:10.1073/pnas.1115495109

Novokhatska, O., Dergai, M., Tsyba, L., Skrypkina, I., Filonenko, V., Moreau, J. and Rynditch, A. (2013). Adaptor proteins intersectin 1 and 2 bind similar proline-rich ligands but are differentially recognized by SH2 domain-containing proteins. *PLoS ONE* **8**, e70546. doi:10.1371/journal.pone.0070546

Obenauer, J. C., Cantley, L. C. and Yaffe, M. B. (2003). Scansite 2.0: proteome-wide prediction of cell signaling interactions using short sequence motifs. *Nucleic Acids Res.* **31**, 3635. doi:10.1093/nar/gkg584

Olivo-Marin, J.-C. (2002). Extraction of spots in biological images using multiscale products. *Pattern Recognit.* **35**, 1989-1996. doi:10.1016/S0031-3203(01)00127-3

Ory, S., Brazier, H. and Blangy, A. (2007). Identification of a bipartite focal adhesion localization signal in RhoU/Wrch-1, a Rho family GTPase that regulates cell adhesion and migration. *Biol. Cell* **99**, 701-716. doi:10.1042/BC20070058

Pagano, A., Crottet, P., Prescianotto-Baschong, C. and Spiess, M. (2004). In Vitro formation of recycling vesicles from endosomes requires adaptor protein-1/clathrin and is regulated by Rab4 and the connector rabaptin-5. *Mol. Biol. Cell* **15**, 4990-5000. doi:10.1091/mbc.e04-04-0355

Praefcke, G. J., Ford, M. G., Schmid, E. M., Olesen, L. E., Gallop, J. L., Peak-Chew, S.-Y., Vallis, Y., Babu, M. M., Mills, I. G. and McMahon, H. T. (2004). Evolving nature of the AP2 α-appendage hub during clathrin-coated vesicle endocytosis. *EMBO J.* **23**, 4371-4383. doi:10.1038/sj.emboj.7600445

Pucharcos, C., Estivill, X. and de la Luna, S. (2000). Intersectin 2, a new multimodular protein involved in clathrin-mediated endocytosis. *FEBS Lett.* **478**, 43-51. doi:10.1016/S0014-5793(00)01793-2

Qin, Y., Meisen, W. H., Hao, Y. and Macara, I. G. (2010). Tuba, a Cdc42 GEF, is required for polarized spindle orientation during epithelial cyst formation. *J. Cell Biol.* **189**, 661-669. doi:10.1083/jcb.201002097

Rink, J., Ghigo, E., Kalaidzidis, Y. and Zerial, M. (2005). Rab conversion as a mechanism of progression from early to late endosomes. *Cell* **122**, 735-749. doi:10.1016/j.cell.2005.06.043

Roberts, M., Barry, S., Woods, A., van der Sluijs, P. and Norman, J. (2001). PDGF-regulated rab4-dependent recycling of αvβ3 integrin from early endosomes is necessary for cell adhesion and spreading. *Curr. Biol.* **11**, 1392-1402. doi:10.1016/S0960-9822(01)00442-0

Rossolillo, P., Winter, F., Simon-Loriere, E., Gallois-Montbrun, S. and Negroni, M. (2012). Retrovolution: HIV-driven evolution of cellular genes and improvement of anticancer drug activation. *PLoS Genet.* **8**, e1002904. doi:10.1371/journal.pgen.1002904

Russo, A. and O'Bryan, J. P. (2012). Intersectin 1 is required for neuroblastoma tumorigenesis. *Oncogene* **31**, 4828-4834. doi:10.1038/onc.2011.643

Ruusala, A. and Aspenström, P. (2008). The atypical Rho GTPase Wrch1 collaborates with the nonreceptor tyrosine kinases Pyk2 and Src in regulating cytoskeletal dynamics. *Mol. Cell. Biol.* **28**, 1802-1814. doi:10.1128/MCB.00201-07

Sakaba, T., Kononenko, N. L., Bacetic, J., Pechstein, A., Schmoranzer, J., Yao, L., Barth, H., Shupliakov, O., Kobler, O., Aktories, K. et al. (2013). Fast neurotransmitter release regulated by the endocytic scaffold intersectin. *Proc. Natl. Acad. Sci. USA* **110**, 8266-8271. doi:10.1073/pnas.1219234110

Saras, J., Wollberg, P. and Aspenström, P. (2004). Wrch1 is a GTPase-deficient Cdc42-like protein with unusual binding characteristics and cellular effects. *Exp. Cell Res.* **299**, 356-369. doi:10.1016/j.yexcr.2004.05.029

Schiavone, D., Dewilde, S., Vallania, F., Turkson, J., Di Cunto, F. and Poli, V. (2009). The RhoU/Wrch1 Rho GTPase gene is a common transcriptional target of both the gp130/STAT3 and Wnt-1 pathways. *Biochem. J.* **421**, 283-292. doi:10.1042/BJ20090061

Shutes, A., Berzat, A. C., Cox, A. D. and Der, C. J. (2004). Atypical mechanism of regulation of the Wrch-1 Rho family small GTPase. *Curr. Biol. CB* **14**, 2052-2056. doi:10.1016/j.cub.2004.11.011

Sigismund, S., Argenzio, E., Tosoni, D., Cavallaro, E., Polo, S. and Di Fiore, P. P. (2008). Clathrin-mediated internalization is essential for sustained EGFR signaling but dispensable for degradation. *Dev. Cell* **15**, 209-219. doi:10.1016/j.devcel.2008.06.012

Simonetti, B. and Cullen, P. J. (2019). Actin-dependent endosomal receptor recycling. *Curr. Opin. Cell Biol.* **56**, 22-33. doi:10.1016/j.ceb.2018.08.006

Sönnichsen, B., De Renzis, S., Nielsen, E., Rietdorf, J. and Zerial, M. (2000). Distinct membrane domains on endosomes in the recycling pathway visualized by multicolor imaging of Rab4, Rab5, and Rab11. *J. Cell Biol.* **149**, 901-914. doi:10.1083/jcb.149.4.901

Stenmark, H., Vitale, G., Ullrich, O. and Zerial, M. (1995). Rabaptin-5 is a direct effector of the small GTPase Rab5 in endocytic membrane fusion. *Cell* **83**, 423-432. doi:10.1016/0092-8674(95)90120-5

Tao, W., Pennica, D., Xu, L., Kalejta, R. F. and Levine, A. J. (2001). Wrch-1, a novel member of the Rho gene family that is regulated by Wnt-1. *Genes Dev.* **15**, 1796-1807. doi:10.1101/gad.894301

Taylor, M. J., Perrais, D. and Merrifield, C. J. (2011). A high precision survey of the molecular dynamics of mammalian clathrin-mediated endocytosis. *PLoS Biol.* **9**, e1000604. doi:10.1371/journal.pbio.1000604

Teyra, J., Huang, H., Jain, S., Guan, X., Dong, A., Liu, Y., Tempel, W., Min, J., Tong, Y., Kim, P. M. et al. (2017). Comprehensive analysis of the human SH3 domain family reveals a wide variety of non-canonical specificities. *Structure* **25**, 1598-1610.e3. doi:10.1016/j.str.2017.07.017

Tsyba, L., Gryaznova, T., Dergai, O., Dergai, M., Skrypkina, I., Kropyvko, S., Boldyryev, O., Nikolaienko, O., Novokhatska, O. and Rynditch, A. (2008). Alternative splicing affecting the SH3A domain controls the binding properties of intersectin 1 in neurons. *Biochem. Biophys. Res. Commun.* **372**, 929-934. doi:10.1016/j.bbrc.2008.05.156

Tsyba, L., Nikolaienko, O., Dergai, O., Dergai, M., Novokhatska, O., Skrypkina, I. and Rynditch, A. (2011). Intersectin multidomain adaptor proteins: regulation of functional diversity. *Gene* **473**, 67-75. doi:10.1016/j.gene.2010.11.016

Vega, F. M. and Ridley, A. J. (2008). Rho GTPases in cancer cell biology. *FEBS Lett.* **582**, 2093-2101. doi:10.1016/j.febslet.2008.04.039

Wandinger-Ness, A. and Zerial, M. (2014). Rab proteins and the compartmentalization of the endosomal system. *Cold Spring Harb. Perspect. Biol.* **6**, a022616. doi:10.1101/cshperspect.a022616

Wong, K. A., Wilson, J., Russo, A., Wang, L., Okur, M. N., Wang, X., Martin, N. P., Scappini, E., Carnegie, G. K. and O'Bryan, J. P. (2012). Intersectin (ITSN) family of scaffolds function as molecular hubs in protein interaction networks. *PLoS ONE* **7**, e36023. doi:10.1371/journal.pone.0036023

Yamabhai, M., Hoffman, N. G., Hardison, N. L., McPherson, P. S., Castagnoli, L., Cesareni, G. and Kay, B. K. (1998). Intersectin, a novel adaptor protein with two Eps15 homology and five Src homology 3 domains. *J. Biol. Chem.* **273**, 31401-31407. doi:10.1074/jbc.273.47.31401

Yang, X., Yan, F., He, Z., Liu, S., Cheng, Y., Wei, K., Gan, S., Yuan, J., Wang, S., Xiao, Y. et al. (2015). ITSN2L interacts with and negatively regulates RABEP1. *Int. J. Mol. Sci.* **16**, 28242-28254. doi:10.3390/ijms161226091

Yu, H., Chen, J. K., Feng, S., Dalgarno, D. C., Brauer, A. W. and Schrelber, S. L. (1994). Structural basis for the binding of proline-rich peptides to SH3 domains. *Cell* **76**, 933-945. doi:10.1016/0092-8674(94)90367-0

Yu, Y., Chu, P.-Y., Bowser, D. N., Keating, D. J., Dubach, D., Harper, I., Tkalcevic, J., Finkelstein, D. I. and Pritchard, M. A. (2008). Mice deficient for the chromosome 21 ortholog Itsn1 exhibit vesicle-trafficking abnormalities. *Hum. Mol. Genet.* **17**, 3281-3290. doi:10.1093/hmg/ddn224

Zamanian, J. L. and Kelly, R. B. (2003). Intersectin 1L guanine nucleotide exchange activity is regulated by adjacent src homology 3 domains that are also involved in endocytosis. *Mol. Biol. Cell* **14**, 1624-1637. doi:10.1091/mbc.e02-08-0494

Zhang, J.-S., Koenig, A., Young, C. and Billadeau, D. D. (2011). GRB2 couples RhoU to epidermal growth factor receptor signaling and cell migration. *Mol. Biol. Cell* **22**, 2119-2130. doi:10.1091/mbc.e10-12-0969